THE JOURNAL OF BIOLOGICAL CHEMISTRY VOL. 282, NO. 1, pp. 216–231, January 5, 2007

Kinetic Mechanism of Human Myosin IIIA*

Received for publication, June 22, 2006, and in revised form, October 23, 2006 Published, JBC Papers in Press, October 29, 2006, DOI 10.1074/jbc.M605964200

Andréa C. Dosé[‡], Shobana Ananthanarayanan[§], Judy E. Moore[§], Beth Burnside[‡], and Christopher M. Yengo[§1]

From the [§]Department of Biology, University of North Carolina, Charlotte, North Carolina 28223 and the [‡]Department of Molecular and Cell Biology, University of California, Berkeley, California 94720

Myosin IIIA is specifically expressed in photoreceptors and cochlea and is important for the phototransduction and hearing processes. In addition, myosin IIIA contains a unique N-terminal kinase domain and C-terminal tail actin-binding motif. We examined the kinetic properties of baculovirus expressed human myosin IIIA containing the kinase, motor, and two IQ domains. The maximum actin-activated ATPase rate is relatively slow (k_{cat} = 0.77 ± 0.08 s^{-1}), and high actin concentrations are required to fully activate the ATPase rate (K_{ATPase} = 34 ± 11 μM). However, actin co-sedimentation assays suggest that myosin III has a relatively high steady-state affinity for actin in the presence of ATP ($K_{actin} \sim 7$ μM). The rate of ATP binding to the motor domain is quite slow both in the presence and absence of actin (K_1k_{+2} = 0.020 and 0.001 $\mu M^{-1}\cdot s^{-1}$, respectively). The rate of actin-activated phosphate release is more than 100-fold faster (85 s^{-1}) than the k_{cat}, whereas ADP release in the presence of actin follows a two-step mechanism (7.0 and 0.6 s^{-1}). Thus, our data suggest a transition between two actomyosin-ADP states is the rate-limiting step in the actomyosin III ATPase cycle. Our data also suggest the myosin III motor spends a large fraction of its cycle in an actomyosin ADP state that has an intermediate affinity for actin ($K_d \sim 5$ μM). The long lived actomyosin-ADP state may be important for the ability of myosin III to function as a cellular transporter and actin cross-linker in the actin bundles of sensory cells.

Molecular motor proteins of the myosin superfamily are capable of converting the energy from ATP hydrolysis into force and motion through a cyclic interaction with actin filaments. Myosins are involved in many different types of cell motility, including muscle contraction, cell division, and intracellular transport (1, 2). Several myosin proteins, including myosins I, III, VI, VIIA, X, and XV, have been found to be involved in sensory processes (3). A common theme emerging from the recent work on the structural and functional properties of myosin motors is that they have a common structural core (4–6), whereas small differences in specific regions alter their kinetic properties, tuning each myosin for its functional role in the cell (7, 8). Thus, understanding the kinetic properties of an uncharacterized myosin protein can provide important insights into its biological function.

Class III myosins were originally discovered in *Drosophila* eyes and designated as the NINAC protein. The electrophysiological response in *Drosophila* eyes lacking the myosin III gene exhibits neither inactivation nor activation following a light stimulus (9). The *ninaC* gene contains an N-terminal kinase domain, a central myosin homology domain, and a C-terminal tail. In addition, localization studies demonstrated that the myosin domain is necessary to concentrate NINAC in the rhabdomere, the microvillus structure that is the site of many steps in phototransduction and contains a filamentous actin core (10). The kinase domain was not required for localization (10). NINAC binds to calmodulin and has the ability to concentrate calmodulin in the rhabdomeres (11). Because calmodulin is thought to be involved in the phototransduction process, concentrating calmodulin may be a major role for myosin III in fly photoreceptors. Other studies have implicated NINAC in the transport of phototransduction signaling proteins such as $G_q\alpha$ (12) and arrestin (13) in a light-dependent manner. Thus myosin III may alter the phototransduction process by modulating the concentration of these important signaling proteins at the site of phototransduction.

Two isoforms of myosin III, myosin IIIA and IIIB, have been identified in humans (14, 15). Myosin IIIA is expressed primarily in the retina and cochlea (14, 15). Myosin IIIA expression has also been found in the retina of striped bass and limulus (16, 17). Mutations in the human myosin IIIA gene have been linked to nonsyndromic deafness (18). Consistent with a role as a cellular transporter, human myosin IIIA containing two IQ domains was found to have ATPase activity, kinase activity, and the ability to move actin filaments in an *in vitro* motility assay (19).

To understand how the myosin III motor functions and is regulated in the cell, it is necessary to determine the kinetic mechanism of its ATPase cycle. The kinetic mechanism provides information about the predominant steady-state intermediates and the duty ratio, the fraction of the ATPase cycle during which myosin is bound to actin. Understanding these kinetic features of myosin III will provide important insights into the mechanism by which this myosin can perform its cellular functions such as intracellular transport or cytoskeletal dynamics. For example, myosin V is a high duty ratio motor and functions as an intracellular transporter by moving processively along actin, taking multiple steps along actin without diffusing away (20, 21). Thus, it can function and is likely regulated as a single molecule (22). Other myosin motors that have a low duty ratio function as a group or as an ensemble of motors, such as in muscle contraction and receptor-mediated endocytosis (8).

* This work was supported by National Institutes of Health Grant R03EY016419, an American Heart Association scientist development grant (to C. M. Y.), and National Institutes of Health Grant EY03575 (to B. B.). The costs of publication of this article were defrayed in part by the payment of page charges. This article must therefore be hereby marked "*advertisement*" in accordance with 18 U.S.C. Section 1734 solely to indicate this fact.

[1] To whom correspondence should be addressed. Tel.: 704-687-8530; E-mail: cmyengo@email.uncc.edu.

Another interesting feature of class III myosins is the N-terminal kinase domain that is capable of autophosphorylating sites on the myosin motor domain (9, 19). It is unclear how this kinase domain plays a role in the phototransduction process or what are its cellular substrates, if there are any. The kinase domain is most similar in sequence to PAK1 kinases (16), which interestingly have been implicated in regulating actin polymerization and myosin activation (23). The kinetics of the kinase domain of myosin III were shown to be quite slow based on the rate of autophosphorylation of sites on the myosin III motor domain (19). In contrast, the kinetics of PAK1 kinases were found to be quite rapid (20–30 s^{-1}) (24). Thus, understanding the kinetics of the myosin III kinase domain may lead to insights into its biological function.

In this study we have expressed and purified human myosin IIIA containing the kinase, motor, and two IQ domains, and we have determined the key individual rate and equilibrium constants in the myosin III motor ATPase cycle. Our results provide important insights into the potential function of myosin III in sensory organs. In addition, our work provides a framework for future studies that will examine the kinetic and biophysical mechanism of myosin III regulation.

EXPERIMENTAL PROCEDURES

Reagents—All reagents were the highest purity commercially available. ATP and ADP were prepared fresh from powder. *N*-Methylanthraniloyl (mant)[2]-labeled 2′-deoxy-ADP and 2′-deoxy-ATP were prepared as described (25, 26) or purchased from Jena Biosciences. The mant-ATP and mant-ADP concentrations were determined from absorbance measurements at 255 nm using ϵ_{255} of 23,300 $M^{-1}\cdot cm^{-1}$. ATP and ADP concentrations were determined by absorbance at 259 nm using ϵ_{259} of 15,400 $M^{-1}\cdot cm^{-1}$. Nucleotides were prepared prior to use in the presence of equimolar $MgCl_2$.

Myosin cDNA Construction and Protein Expression and Purification—We generated a construct of human myosin IIIA truncated after the second IQ domain (residues 1–1143) (MIII), and containing a C-terminal FLAG tag (DYKDDDDK) for purification purposes (27–30). Recombinant baculoviruses of myosin III and calmodulin generated with the FastBac system (Invitrogen) were co-expressed in Sf9 cells. The purity was assessed with Coomassie-stained SDS gels. Myosin concentrations were determined using the Bio-Rad microplate assay using bovine serum albumin as a standard (29, 30). Absorbance measurements were also performed, and a predicted extinction coefficient of 129,500 $M^{-1}\cdot cm^{-1}$ was used to calculate the concentration with similar results. Actin was purified from rabbit skeletal muscle using an acetone powder method (31). Pyrene actin was generated by labeling actin with pyrene iodoacetamide (Molecular Probes) as described (32). All experiments were performed in KMg50 buffer (50 mM KCl, 1 mM EGTA, 1 mM $MgCl_2$, 1 mM dithiothreitol, and 10 mM imidazole-HCl, pH 7.0, 25 °C).

Steady-state ATPase Activity of MIII—Steady-state ATP hydrolysis by MIII (50–100 nM) in the absence and presence of actin (0–70 μM) was examined using the NADH-linked assay (28–30) with a final MgATP concentration of 1 mM.

Kinase Activity—Autophosphorylation of the MIII was detected by Western blot analysis using anti-phosphothreonine antibodies. MIII (0.5 μM) was allowed to react with ATP for specific time periods ranging from 10 s to 60 min. The reaction was stopped at each time point by the addition of SDS loading buffer. A series of time course experiments was conducted at various ATP concentrations (0–1000 μM). Samples from sequential time points for each specific ATP concentration were run on SDS-PAGE, transferred to nitrocellulose membrane, blocked with 3% bovine serum albumin and probed with anti-phosphothreonine primary antibodies (Zymed Laboratories Inc.). Anti-rabbit horseradish peroxidase-linked IgG (Cell Signaling Technology) was applied as the secondary antibody, followed by treatment with Lumiglo chemiluminescence reagent (Cell Signaling Technology) to detect the bands of phosphorylated protein with x-ray film. Densitometry analysis using NIH image software was used to determine the band intensities. The membrane was subsequently stripped and reprobed with an anti-FLAG antibody to detect total protein and verify even loading of samples.

Kinase activity was also examined by performing time courses as described above using [γ-^{32}P]ATP as a substrate. The number of moles of ^{32}P incorporated into each mole of MIII was determined by subjecting each sample of the time course to SDS-PAGE, excising each band, and dissolving the bands in 30% H_2O_2. The dissolved bands were examined by scintillation counting and compared with a standard curve to determine the moles of ^{32}P incorporated per mol of MIII.

Actin Co-sedimentation Assay—MIII was equilibrated with actin (0–60 μM) and the ATP-regeneration system (2 mM phosphoenolpyruvate and 20 units/ml pyruvate kinase). 2 mM ATP was added just prior to ultracentrifugation in a TLA 100.2 Beckman centrifuge at 320,000 × *g* for 20 min at 25 °C. The ADP concentration in the supernatant was determined by mixing a specified amount of the supernatant with the NADH mix and measuring the change in NADH absorbance as described under "Steady-state ATPase Activity." Equal amounts of the supernatant and pellet were subjected to SDS-PAGE, and the fraction of MIII bound to actin was determined by quantifying the amount of MIII in the supernatant and pellet with densitometry using NIH image software. The fraction bound was plotted as a function of actin concentration to determine the affinity of myosin III for actin in the presence of ATP.

Fluorescence Spectroscopy—A Quantamaster fluorimeter (Photon Technology International, Lawrenceville, NJ) equipped with a 75-watt xenon arc lamp as an excitation source and excitation/emission monochromators was used to measure steady-state fluorescence of pyrene actin. Pyrene actin was excited at 365 nm, and the emission spectra was measured from 380 to 550 nm. Slit widths were set at a resolution of 1 nm. All fluorescence spectra were corrected for variations in the wavelength sensitivity of the detector system, the presence of Raman scatter, and background fluorescence in the appropriate buffer solution.

Acid Quench—To determine the equilibrium constant for ATP hydrolysis, 0.9 μM myosin III was mixed with 25 μM ATP

[2] The abbreviations used are: mant, *N*-methylanthraniloyl; MDCC-PBP, *N*-[2-(1-maleimidyl)ethyl]-7-(diethylamino)coumarin-3-carboxamide.

$$\begin{array}{ccccccccccccc}
 & & K_1' & & K_2' & & K_3' & & K_4' & & K_{5A}' & & K_{5B}' & \\
\mathbf{AM} & \leftrightarrow & \mathbf{AM(ATP)} & \leftrightarrow & \mathbf{AM.ATP} & \leftrightarrow & \mathbf{AM.ADP.Pi} & \leftrightarrow & \mathbf{AM.ADP'} & \leftrightarrow & \mathbf{AM.ADP} & \leftrightarrow & \mathbf{AM} \\
K_6\uparrow\downarrow & & K_7\uparrow\downarrow & & K_8\uparrow\downarrow & & K_9\uparrow\downarrow & & K_{10A}\uparrow\downarrow & & K_{10B}\uparrow\downarrow & & K_6\uparrow\downarrow \\
\mathrm{M} & \leftrightarrow & \mathrm{M(ATP)} & \leftrightarrow & \mathbf{M.ATP} & \leftrightarrow & \mathbf{M.ADP.Pi} & \leftrightarrow & \mathrm{M.ADP'} & \leftrightarrow & \mathrm{M.ADP} & \leftrightarrow & \mathrm{M} \\
 & & K_1 & & K_2 & & K_3 & & K_4 & & K_{5A} & & K_{5B} &
\end{array}$$

SCHEME 1

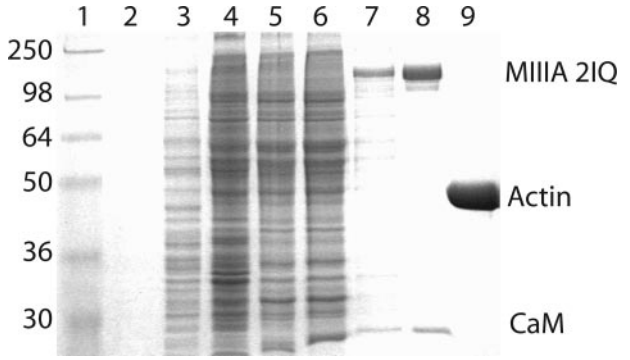

FIGURE 1. **SDS-PAGE of purified myosin III.** Samples from each step of the purification process are shown compared with the molecular weight marker and actin. Lanes are as follows: *lane 1,* molecular weight markers; *lane 3,* cell lysate ultracentrifuge pellet; *lane 4,* ultracentrifuge supernatant; *lane 5,* flow-through from FLAG column; *lane 6,* wash from FLAG column; *lane 7,* elute from FLAG column; *lane 8,* after final $(NH_4)_2SO_4$ cut, *lane 9*) G-actin. *CaM*, calmodulin.

containing [γ-^{32}P]ATP, allowed to react at 25 °C for 1–20 s, and quenched with quench solution (2 N HCl, 0.35 M KH_2PO_4). The hydrolyzed [γ-^{32}P]ATP was separated from unhydrolyzed [γ-^{32}P]ATP using activated charcoal, and scintillation counting was used to determine [γ-^{32}P]ATP concentrations (33, 34). The number of moles of [γ-^{32}P]ATP hydrolyzed per mol of myosin was used to calculate the phosphate burst and the equilibrium constant for hydrolysis.

Stopped-flow Measurements and Kinetic Modeling—Transient kinetic experiments were performed in an Applied Photophysics stopped-flow with a dead time of 1.2 ms. A monochromator with a 2 nm band pass was used for fluorescence excitation, and cut-off filters were used to measure the emission. All optical filters were provided with the stopped-flow instrument. Light scatter was measured at 320 nm at 90° with a 305 nm long pass filter. Pyrene actin was excited at 365 nm, and the emission was measured using a 400 nm long pass filter. Mant-labeled nucleotides were excited by energy transfer from tryptophans by exciting at 295 nm or by direct excitation at 355 nm, and the emission was measured through a 400 nm long pass filter. Both methods of exciting mant-ATP and mant-ADP gave similar results. Nonlinear least squares fitting of the data were done with software provided with the instrument or Kaleidagraph (Synergy Software, Reading, PA). Uncertainties reported are standard error of the fits unless stated otherwise.

The kinetics of phosphate release were measured using phosphate-binding protein covalently labeled with *N*-[2-(1-maleimidyl)ethyl]-7-(diethylamino)coumarin-3-carboxamide (MDCC-PBP) (generously provided by Howard White, Eastern Virginia University School of Medicine) (35). The fluorescence of MDCC-PBP, which increases severalfold in the presence of inorganic phosphate (35, 36), was excited at 400 nm, and the emission was measured through a 425 nm long pass filter. Phosphate release was measured with a sequential mix experiment in which 2 μM myosin III was mixed with 1.75 μM ATP and aged for 5 s to allow myosin III to bind and hydrolyze the ATP, and then the MIII·ADP·P_i complex was mixed with actin (0–40 μM) (29, 36) (final concentrations after mixing 1.0 μM MIII, 0.875 μM ATP, 2.7 μM MDCC-PBP). All solutions were preincubated with 7-methylguanosine (0.2 mM) and purine nucleoside phosphorylase (0.2 units·ml^{-1}) to remove background phosphate.

Kinetic modeling and simulations were performed with Pro-K software (Applied Photophysics) using the reaction scheme, which has recently been used in kinetics studies of myosin V, VI ,and VII (20, 28–30, 37–39) (see Scheme 1). In Scheme 1, myosin, actin, and actomyosin are represented by M, A, and AM, respectively. The rate and equilibrium constants are labeled on the basis of the reaction proceeding from left to right and those between the actin-associated and-dissociated steps proceeding in the dissociated direction. The main flux of the reaction pathway is shown in boldface. All concentrations mentioned in the stopped-flow experiments are final concentrations unless stated otherwise.

RESULTS

Protein Expression and Purification—The expression yields of human myosin IIIA 2IQ co-expressed with calmodulin (MIII) in the baculovirus insect cell (Sf9) system were ~0.5–1 mg/liter of Sf9 cells at a density of 2.0×10^6 cells/ml. The purity of MIII following anti-FLAG affinity chromatography was ~95% based on Coomassie-stained SDS-polyacrylamide gels (Fig. 1). The stoichiometry of calmodulin to MIII in the final purified product was determined to be two calmodulins per myosin with densitometry analysis of SDS-polyacrylamide gels (data not shown). All experiments were performed in KMg50 and in the presence of 10 μM calmodulin to ensure the IQ domains of MIII had bound calmodulin.

Steady-state ATPase Activity—We examined the actin-activated ATPase activity of MIII using the NADH-coupled assay in KMg50 buffer at 25 °C (Fig. 2*A*). The rate of ATPase activity was plotted as a function of actin concentration and the data fit to the Michaelis-Menten relationship. The maximum rate of ATPase activity (k_{cat}) was found to be 0.77 ± 0.06 s^{-1}, and the actin concentration at which one-half-maximal activity was achieved (K_{ATPase}) was found to be 34 ± 11 μM.

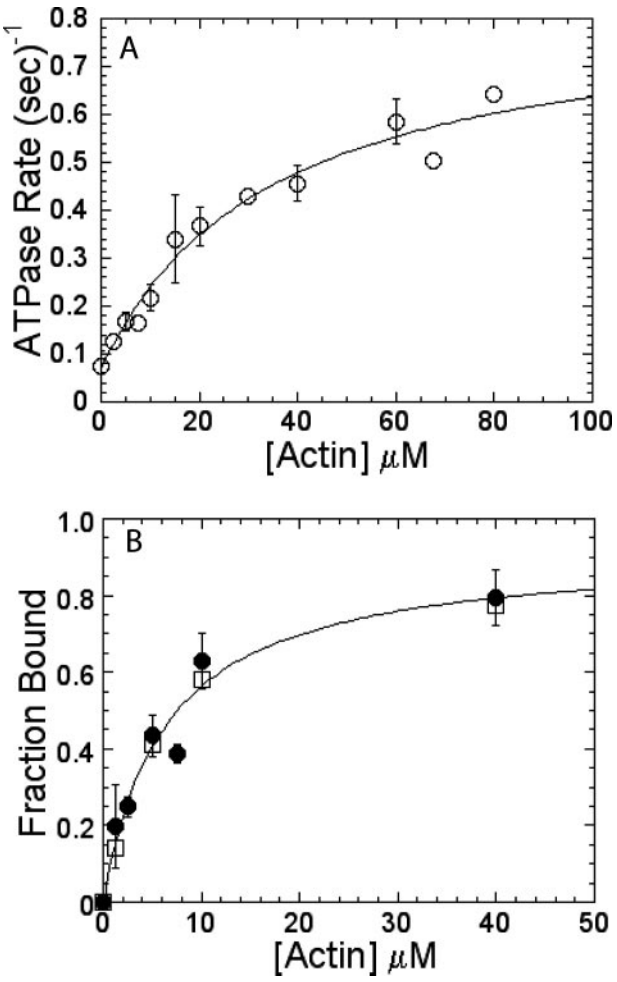

FIGURE 2. **ATPase activity and actin binding affinity of myosin III.** *A,* steady-state ATPase rate was measured using the NADH coupled assay in the presence of various concentrations of actin. The k_{cat} and K_{ATPase} values were determined by fitting the data to the Michaelis-Menten equation, and v_0 is the ATPase activity in the absence of actin. *B,* the affinity of myosin III for F-actin was measured with the actin co-sedimentation assay. Myosin III (0.9 μM) was equilibrated in the presence of various concentrations of actin, 2 mM ATP, and the ATP-regeneration system and then pelleted at 25 °C. The fraction of myosin III bound to actin was quantified by performing densitometry on Coomassie-stained gels following SDS-PAGE. The plot of the fraction bound (*closed circles*) as a function of actin concentration was fit to a hyperbola to determine the steady-state affinity for actin. The fraction bound was also calculated with kinetic simulations (*open squares*) performed with the described rate and equilibrium constants (Table 2). The *error bars* represent the standard deviation from three separate experiments done with different protein preparations.

Single turnover experiments were performed with mant-ATP, which enhances its fluorescence when bound to myosin, to monitor the turnover rate of MIII in the presence and absence of actin (data not shown). MIII (1.0 μM) was mixed with 25 μM mant-ATP, aged for 10 s, and then mixed with 0.5 mM unlabeled ADP in the presence and absence of 20 μM actin (final reaction conditions: 0.5 μM MIII, 12.5 μM mant-ATP, 0.5 mM ADP, with and without 20 μM actin). The decrease in mant fluorescence was monitored as a function of time. The fluorescence transients were biexponential with a fast phase of 16 ± 1 s^{-1} and a slow phase of 0.11 ± 0.01 s^{-1} (relative amplitudes = 0.62 and 0.38, respectively) in the absence of actin, and a fast phase of 18 ± 1 s^{-1} and slow phase of 0.78 ± 0.15 s^{-1} (relative amplitudes = 0.57 and 0.43, respectively) in the presence of actin. The fast phase was modeled to be mant-ATP dissociation from the kinase domain, determined from the direct binding experiments described below (Fig. 4), whereas the slow phase was modeled to be the rate of ATP turnover by the motor domain. The slow phase of the fluorescence transient is in relatively good agreement with the steady-state ATPase rate in the absence of actin and the k_{cat} in the presence of actin (Table 1).

TABLE 1
Steady-state parameters of the MIII motor ATPase cycle

Steady-state parameters	Value
v_0 $(s)^{-1}$ [a]	0.07 ± 0.03
v_0 $(s)^{-1}$ [b]	0.11 ± 0.01
k_{cat} $(s)^{-1}$ [c]	0.77 ± 0.08
k_{cat} $(s)^{-1}$ [b]	0.78 ± 0.15
K_{ATPase} (μM)[d]	34 ± 11
K_{actin} (μM)[e]	7.0 ± 0.6

[a] Steady-state ATPase activity in the absence of actin measured with the NADH-coupled assay.
[b] Single turnover measurement with mant-ATP.
[c] Maximum rate of actin-activated ATPase measured with the NADH-coupled assay. The values for K_{ATPase} and k_{cat} were determined from the fit of the data in Fig. 2 to the following equation: $(v_0 + (k_{cat}[actin])/(K_{ATPase} + actin))$.
[d] Actin concentration at which the actin-activated ATPase rate is one-half-maximal from the NADH assay.
[e] Dissociation constant of myosin III for F-actin in the presence of ATP and ATP-regeneration system, measured by actin co-sedimentation.

Actin Affinity in the Presence of ATP—Actin co-sedimentation assays were performed to determine the affinity of MIII for actin in the presence of ATP and the ATP-regeneration system. The ADP concentration in the supernatant following centrifugation at 25 °C was determined by NADH absorbance as in the steady-state ATPase assay. The ADP concentration was determined to be less than 10% of the total nucleotide concentration. Fig. 2*B* demonstrates the fraction of MIII bound to actin as a function of actin concentration. The data were fit to a hyperbola to determine the actin affinity in the presence of ATP (K_{actin} = 7.0 ± 0.6 μM) and a maximum fraction bound of 0.91 ± 0.1. In addition, the data were compared with a simulation of the fraction of myosin III bound to actin determined from the rate and equilibrium constants described below (Table 2).

Kinase Domain Activity—The rate of autophosphorylation in MIII was monitored by examining the time course of phosphothreonine incorporation following the addition of ATP using quantitative Western blotting and radiolabeled ATP, [γ-^{32}P]ATP (see "Experimental Procedures") (Fig. 3). The phosphorylation time courses were found to have an initial linear phase followed by saturation after 10–30 min (Fig. 3*A*, single exponential fit, k_{obs} = 0.46 ± 0.07 min^{-1}; linear phase = 0.67 ± 0.05 min^{-1}). The rate of the initial phase was linearly dependent on ATP concentration from 50–1000 μM ATP (Fig. 3*B*, 0.001 ± 0.0001 $\mu M^{-1}\cdot min^{-1}$). Experiments were performed in parallel using [γ-^{32}P]ATP (200 μM) to determine the number of moles of ^{32}P incorporated into MIII upon saturation (Fig. 3*C*). We found 2.2 ± 0.2 moles of phosphate were incorporated into each mole of MIII during the course of the reaction. The results of these experiments suggest the overall kinase autophosphorylation reaction is quite slow (0.002 mol of P_i·mol of myosin$^{-1}\cdot s^{-1}$ at 200 μM ATP), and phosphorylation of threonine is linearly dependent on ATP concentration from 0 to 1000 μM ATP.

TABLE 2
Summary of rate and equilibrium constants in the myosin IIIA motor ATPase cycle

ATP binding and hydrolysis	
K_1k_{+2} ($\mu M^{-1}\cdot s^{-1}$)[a]	0.010 ± 0.004
K_1k_{+2} ($\mu M^{-1}\cdot s^{-1}$)[b]	0.003 ± 0.001
K_3[c]	9
$K_1'k_{+2}'$ ($\mu M^{-1}\cdot s^{-1}$)[a]	0.005 ± 0.002
$K_1'k_{+2}'$ ($\mu M^{-1}\cdot s^{-1}$)[b]	0.043 ± 0.010
$K_1'k_{+2}'$ ($\mu M^{-1}\cdot s^{-1}$)[d]	0.022 ± 0.001
$1/K_1'$ (μM)[d]	11,144 ± 2319
k_{+2}' (s^{-1})[d]	246 ± 38
ADP binding	
k_{+5B} (s^{-1})[e]	6.8 ± 0.2
k_{-5B}' ($\mu M^{-1}\cdot s^{-1}$)[e]	1.0 ± 0.1
$1/K_{5B}'$ (μM)[e]	6.8 ± 0.4
k_{+5A}' (s^{-1})[e]	0.60 ± 0.10
k_{+5A}' (s^{-1})[f]	0.97 ± 0.03
k_{-5A}' (s^{-1})[f]	0.54 ± 0.08
K_{5A}'[f]	1.8 ± 0.3
k_{+5B}' (s^{-1})[f]	9.84 ± 0.25
k_{-5B}' ($\mu M^{-1}\cdot s^{-1}$)[f]	0.29 ± 0.11
$1/K_{5B}'$ (μM)[f]	34 ± 14
k_{+5A} (s^{-1})[f]	1.00 ± 0.24
k_{-5A} (s^{-1})[f]	0.88 ± 0.11
K_{5A}[f]	1.1 ± 0.3
k_{+5B} (s^{-1})[f]	9.26 ± 1.55
k_{-5B} ($\mu M^{-1}\cdot s^{-1}$)	0.31 ± 0.09
$1/K_{5B}$ (μM)[f]	30 ± 11
P_i release	
k_{+4}' (s^{-1})[g]	85 ± 17
$1/K_9$ (μM)[g]	44 ± 15
Actin binding	
k_{+6} ($\mu M^{-1}\cdot s^{-1}$)[h]	11.4 ± 0.4
k_{-6} (s^{-1})[h]	1.5 ± 0.1
$1/K_6$ (μM)[h]	0.13 ± 0.01
$1/K_6$ (μM)[i]	0.06 ± 0.02
k_{+10B} ($\mu M^{-1}\cdot s^{-1}$)[h]	14.6 ± 0.6
k_{-10B} (s^{-1})[h]	1.2 ± 0.1
$1/K_{10B}$ (μM)[h]	0.08 ± 0.01
$1/K_{10B}$ (μM)[i]	0.06 ± 0.03
$1/K_{10A}$ (μM)[j]	5.0

[a] mant-ATP fluorescence.
[b] ATP binding by competition with mant-ATP.
[c] Acid quench with [γ-^{32}P]ATP.
[d] ATP-induced dissociation was monitored by light scatter.
[e] ADP competition with ATP-induced dissociation was monitored by light scatter.
[f] mant-ADP fluorescence.
[g] Phosphate-binding protein.
[h] Pyrene actin fluorescence, association, and dissociation.
[i] Pyrene actin fluorescence, titration.
[j] Data were predicted from kinetic simulation.

The rate of autophosphorylation with mant-ATP (100 μM) as a substrate was similar to that with ATP at the same concentration (data not shown). However, the maximum level of phosphorylation was reduced 2-fold with mant-ATP compared with ATP. These results indicate that the mant fluorophore reduces the affinity of the kinase domain for ATP but does not alter autophosphorylation activity.

ATP Binding—To determine the kinetics of ATP binding to myosin III, we used fluorescently labeled ATP (mant-ATP), which was modeled with Reaction 1 (where mant-ATP* indicates enhanced mant fluorescence) (Fig. 4).

$$M + mATP \overset{K_1}{\longleftrightarrow} M(mATP) \overset{K_2}{\longleftrightarrow} M\cdot mATP^*$$

$$AM + mATP \overset{K_1'}{\longleftrightarrow} AM(mATP) \overset{K_2'}{\longleftrightarrow} AM\cdot mATP^*$$

REACTION 1

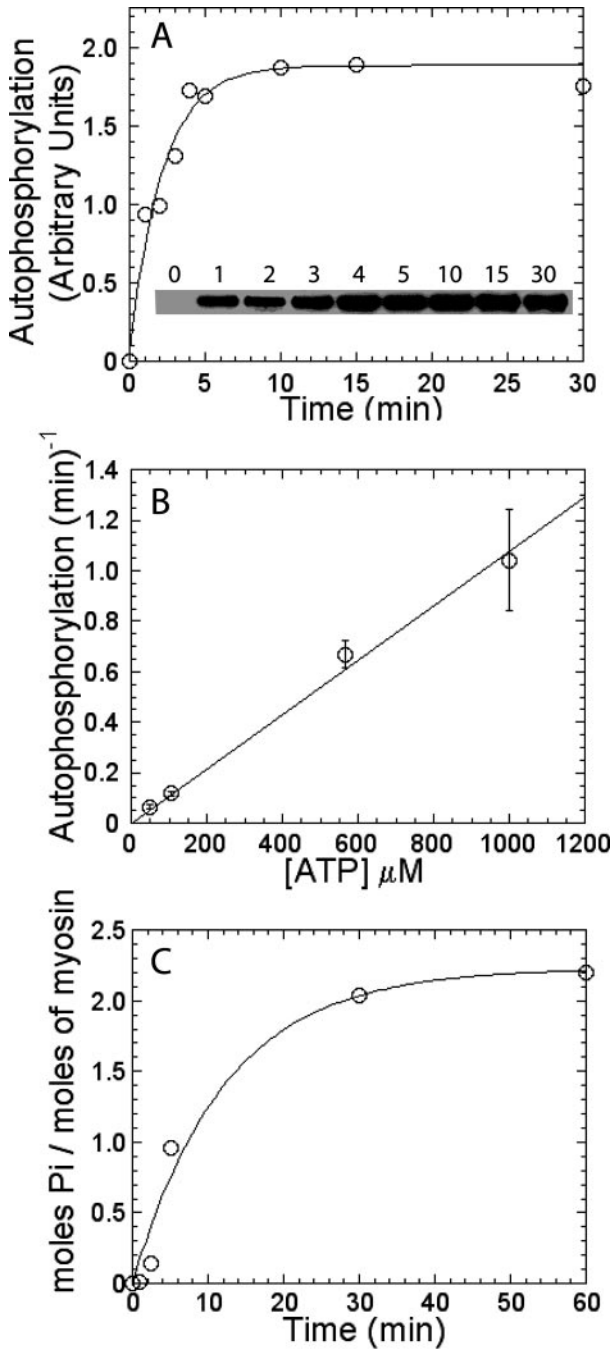

FIGURE 3. **Myosin III kinase activity.** *A,* rate of autophosphorylation was monitored by examining phosphothreonine content by Western blotting with anti-phosphothreonine antibodies. Samples were incubated with ATP and quenched with SDS loading buffer at specific time points after the addition of ATP. Densitometry was used to quantify the increase in phosphothreonine as a function of time. The time course from an experiment with 565 μM ATP is shown, and the data are fit to a single exponential function (k_{obs} = 0.46 ± 0.07 min^{-1} and linear phase = 0.67 ± 0.05 min^{-1}). *Inset* shows the Western blotting results; each lane is labeled with the incubation time in minutes. *B,* initial linear phase of the time course allowed us to determine the autophosphorylation rate at each ATP concentration. The plot demonstrates that autophosphorylation rate (min^{-1}) is linearly dependent on ATP concentration in the concentration range measured (linear fit = 0.0010 ± 0.0001 $\mu M^{-1}\cdot min^{-1}$). *C,* the kinase activity was also measured with a similar experiment, but using [γ-^{32}P]ATP (200 μM) to determine the total amount of phosphate incorporation at each time point. The amount of ^{32}P incorporation as a function of time was fit to a single exponential function (k_{obs} = 0.082 ± 0.02 min^{-1}, linear phase = 0.16 ± 0.03 min^{-1}) to determine the maximum number of moles of ^{32}P per mol of myosin III (2.2 ± 0.2).

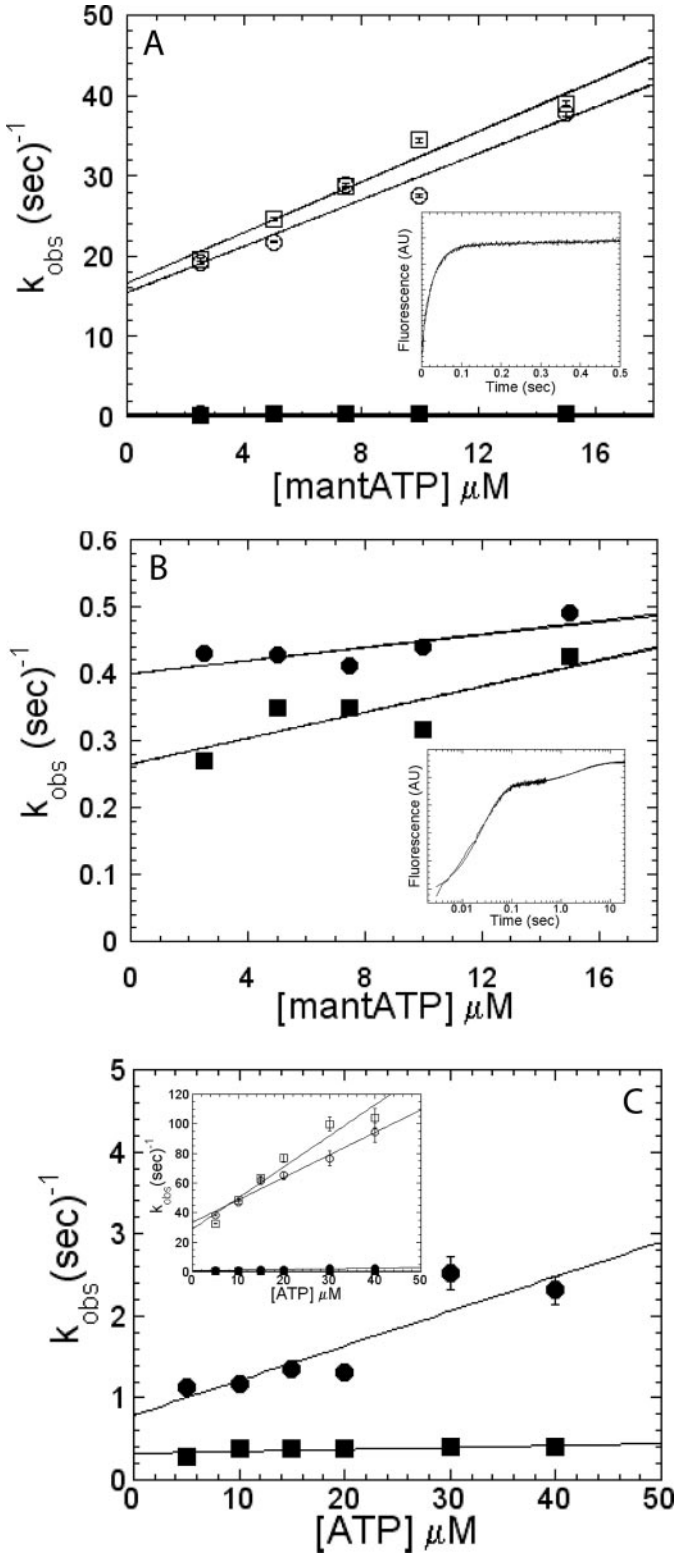

FIGURE 4. **The rate of mant-ATP binding to myosin III (0.5 μM) and actomyosin III (0.5 μM MIII; 2 μM actin) monitored with mant-ATP fluorescence.** The fluorescence transients were fit to a two-exponential function at all mant-ATP concentrations. The relative amplitudes of the fast and slow phases were similar at each mant-ATP concentration measured but slightly different in the presence (amplitudes, fast = 0.80 and slow = 0.20) and absence (amplitudes, fast = 0.86 and slow = 0.14) of actin. *A*, the fast phases of the fluorescence transients were linearly dependent on mant-ATP concentration in the presence (*open circles*) and absence (*open squares*) of actin and were assigned to the kinase domain. The *inset* demonstrates the fast phase of the fluorescence transient at 15 μM mant-ATP (k_{obs} = 37.8 ± 0.3 s^{-1}). *B*, the slow phases were also linearly dependent on mant-ATP concentrations in the presence (*closed circles*) and absence (*closed squares*) of actin and were assigned to the motor domain. The data were fit to a linear regression to determine the second-order rate constant for mant-ATP binding to MIII in the absence (K_1k_{+2}) and presence ($K_1'k_{+2}'$) of actin. The *inset* demonstrates the slow phase of the fluorescence transient at 15 μM mant-ATP plotted on a log scale (k_{obs} = 0.43 ± 0.3 s^{-1}). *C*, the rate of ATP binding was also measured by kinetic competition with mant-ATP (see "Results"). Myosin III (1 μM) or actomyosin III (1 μM MIII: 2 μM actin) was mixed with 5 μM mant-ATP and varying concentrations of ATP. The fast (MIII, *open squares*; actomyosin III, *open circles*) and slow phases (MIII, *closed squares*; actomyosin III, *closed circles*) both increased linearly as a function of ATP concentration, which allowed us to determine the second-order rate constant for ATP binding to the motor and kinase domains (see Table 2). The *inset* shows the rate constants for the fast phase of the fluorescence transient measured as a function of ATP concentration.

The rate of the mant-ATP fluorescence increase as a function of time was fit to a two-exponential function at each mant-ATP concentration in the presence and absence of actin. The fast and the slow phases of the fluorescence transients were both linearly dependent on mant-ATP concentration. The fast phase of the fluorescence transient was found to have a similar second-order binding constant in the presence (1.6 ± 0.2 μM^{-1}·s^{-1}) and absence of actin (1.5 ± 0.2 μM^{-1}·s^{-1}) (Fig. 4*A*). The slow phase of the fluorescence transient changed very little in the mant-ATP concentration range measured, and thus it was difficult to fit the data to a linear relationship. Nevertheless, the linear fit of the data gave an estimate of the second-order rate constants in the presence ($K_1'k_{+2}'$ = 0.005 ± 0.002 μM^{-1}·s^{-1}) and absence (K_1k_{+2} = 0.010 ± 0.004 μM^{-1}·s^{-1}) of actin (Fig. 4*B*). The relative amplitudes of the fast and slow phases in the absence and presence of actin (0.86, 0.14, 0.8, and 0.2, respectively) were similar at all mant-ATP concentrations measured. The data from the fast phase contain a *y* intercept of ~16 s^{-1}, whereas the slow phase contains a much lower intercept in the presence and absence of actin (0.40 ± 0.02 and 0.26 ± 0.03 s^{-1}). By comparing these data with the ATP-induced dissociation of actomyosin III experiments (Fig. 5) and mant-ATP competition experiments (Fig. 4*C*) described below, the slow phase was assigned to mant-ATP binding to the motor and the fast phase was assigned to mant-ATP binding to the kinase domain.

To determine the kinetics of unlabeled ATP binding to myosin and actomyosin III, we examined ATP binding by kinetic competition with mant-ATP (Reaction 2) (Fig. 4*C*) (34, 38).

$$\begin{array}{ccccc} & & K_1 & & K_2 \\ \mathrm{M} + \mathrm{mATP} & \longleftrightarrow & \mathrm{M(mATP)} & \longleftrightarrow & \mathrm{M \cdot mATP^*} \\ + & & & & \\ \mathrm{ATP} & & & & \\ K_1 \uparrow\downarrow & & & & \\ \mathrm{M(ATP)} & & & & \\ K_2 \uparrow\downarrow & & & & \\ \mathrm{M \cdot ATP} & & & & \end{array}$$

REACTION 2

MIII or actomyosin III was mixed with 5 μM mant-ATP and varying concentrations of ATP. The fluorescence transients were biphasic with slow and fast phases that were linearly dependent on ATP concentration. In the absence of actin, the

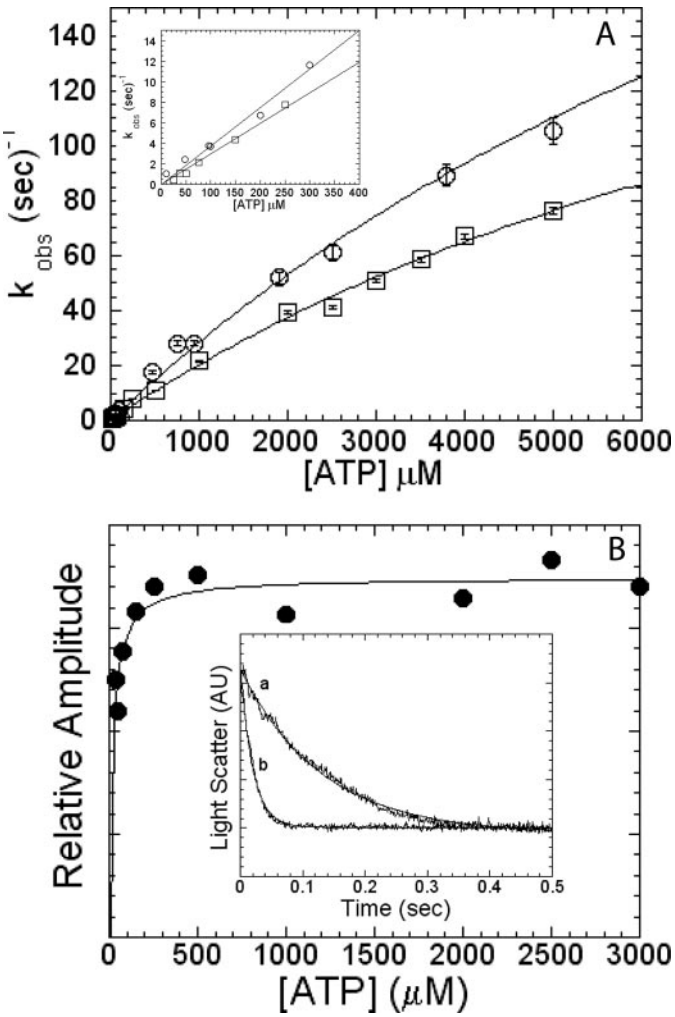

FIGURE 5. **The rate of ATP binding to 0.5 μM actomyosin III monitored by pyrene actin (*open circles*) fluorescence or light scattering (*open squares*).** *A*, rate of ATP binding was found to be hyperbolically dependent on ATP concentration for both the pyrene actin and light scatter signals. The data were fit to a hyperbola to determine the second-order rate constant ($K_1'k_{+2}'$), equilibrium constant (K_1'), and maximum rate (k_{+2}') for ATP binding. *Inset* is the rates of binding measured at low ATP concentrations (0–400 μM). *B*, light scatter signal decreased upon ATP binding, and the amplitude of the decrease was plotted as a function of ATP concentration. A hyperbolic fit of the amplitude data was used to determine the apparent affinity of actomyosin III for ATP (19.5 ± 3.4 μM). The *inset* shows the light scatter transients and the single exponential fits of the data from two different ATP concentrations as follows: (*a*) 250 μM ATP (k_{obs} = 21.1 ± 0.2 s^{-1}; (*b*) 3000 μM ATP (k_{obs} = 50.8 ± 0.5 s^{-1}).

slow phase was fit to a second-order binding constant of 0.003 ± 0.001 $\mu M^{-1}\cdot s^{-1}$, whereas the fast phase was fit to a second-order binding constant of 2.1 ± 0.3 $\mu M^{-1}\cdot s^{-1}$. In the presence of actin, the second-order binding constant of the slow phase was 10-fold faster than in the absence of actin (0.042 ± 0.01 $\mu M^{-1}\cdot s^{-1}$), whereas the fast phase was similar (1.5 ± 0.1 $\mu M^{-1}\cdot s^{-1}$). The slow phase for ATP binding in the presence of actin was faster than that determined with mant-ATP, indicating the mant fluorophore reduces the rate of ATP binding in the presence of actin. The slow phase in the presence of actin was similar to the second-order binding constant for ATP binding to the motor domain as determined with pyrene actin and light scatter (Fig. 5).

We examined the rate of ATP binding specifically to the motor domain using pyrene-labeled actin, which allowed us to assign the two phases from the previous ATP binding experiments to the motor and kinase domains. Strongly bound myosin quenches pyrene actin, and upon ATP binding the fluorescence recovers because of population of the weakly bound states of myosin. The ATP-induced rate of formation of weakly bound actomyosin III (0.5 μM) was monitored as shown in Reaction 3, where A* indicates unquenched pyrene actin fluorescence (Fig. 5*A*).

$$\mathrm{AM} + \mathrm{ATP} \overset{K_1'}{\longleftrightarrow} \mathrm{AM(ATP)} \overset{K_2'}{\longleftrightarrow} \mathrm{A^*M \cdot ATP} \overset{K_8'}{\longleftrightarrow} \mathrm{A^* + M \cdot ATP}$$

REACTION 3

The linear fit of the ATP binding rates as a function of ATP concentration (in the concentration range of 0–2000 μM ATP) was used to determine the second-order rate constant for ATP binding ($K_1'k_{+2}'$). The second-order rate constant for ATP binding to MIII was found to be ~6-fold faster ($K_1'k_{+2}'$ = 0.034 ± 0.003 $\mu M^{-1}\cdot s^{-1}$) than the slow phase observed with mant-ATP and similar to that measured with the mant-ATP competition experiment (Fig. 4*C*). However, ATP binding was nearly 100-fold slower than the fast phase of that measured with mant-ATP. Thus, the slow phase from the mant-ATP binding experiments was assigned to the motor domain, and the fast phase was assigned to the kinase domain. The hyperbolic fit of the data allowed us to determine the equilibrium constant ($1/K_1'$ = 7500 ± 1800 μM), as well as the maximum rate of ATP binding (k_{+2}' = 259 ± 44 s^{-1}) to pyrene actomyosin III.

Similar experiments were performed with unlabeled F-actin by using the light scatter signal to monitor ATP-induced dissociation of actomyosin III. The second-order rate constant for ATP binding to actomyosin III was found to be slightly slower than that measured with pyrene actin ($K_1'k_{+2}'$ = 0.022 ± 0.001 $\mu M^{-1}\cdot s^{-1}$). The equilibrium constant for ATP binding to actomyosin III was weaker than that measured with pyrene actin ($1/K_1'$ = 11,144 ± 2319 μM). Finally, the maximum rate of ATP-induced dissociation was similar (k_{+2}' = 246 ± 38 s^{-1}) to that measured with pyrene actin. The amplitudes of the light scatter transients were plotted as a function of ATP concentration, which allowed us to determine the apparent affinity of actomyosin III for ATP (K_d = 19.5 ± 3.4 μM) (Fig. 5*B*). The apparent affinity can be modeled with the equation $K_d = K_1'k_{+2}'/k_{-2}'$, which assumes the initial interaction is a rapid equilibrium (K_1') that is followed by an isomerization step (K_2'). These results suggest that the rate of the isomerization from the weakly bound to the strongly bound conformation (K_2') limits the overall rate of ATP-induced dissociation of myosin III from actin. Based on the ATP binding rates that pass relatively close to the origin and the slow rate of the reverse isomerization step estimated from the above equation (k_{-2}' = 0.001 s^{-1}), we conclude that ATP binding to the motor domain is essentially irreversible.

ATP Hydrolysis—The equilibrium constant for ATP hydrolysis was determined by acid quench experiments with

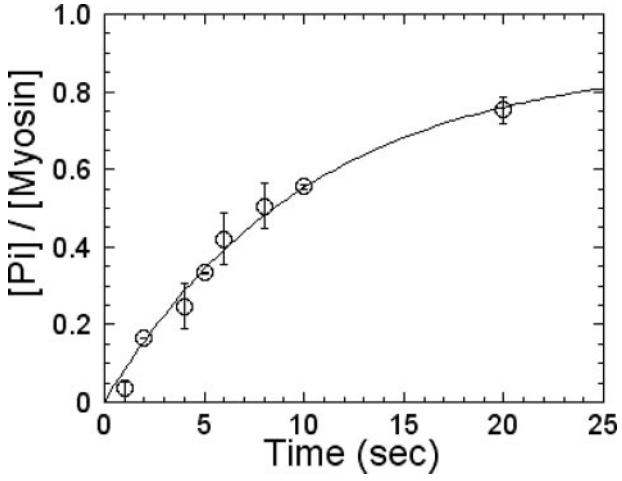

FIGURE 6. **The equilibrium constant for ATP hydrolysis determined by acid quench experiments.** Myosin III (0.9 μM) was mixed with [γ-^{32}P]ATP (25 μM) and allowed to age for specific time points (1–20 s) before manually quenching the reaction with acid. The amount of ^{32}P and thus the amount of ATP hydrolyzed was determined as described under "Experimental Procedures." The data were fit to an exponential function with a rate constant of 0.10 $\pm$ 0.01 s^{-1} and a burst of 0.89 $\pm$ 0.06 μM P_i per μM myosin III. The value of 0.1 s^{-1} is similar to the rate of ATP binding to the motor domain at 25 μM ATP suggesting the reaction was essentially limited by ATP binding to the motor domain.

[γ-^{32}P]ATP (see "Experimental Procedures") (Fig. 6). After mixing 25 μM [γ-^{32}P]ATP with 0.9 μM MIII, the reaction was quenched at time points from 1 to 20 s. The amount of ATP hydrolyzed per myosin was plotted as a function of time in Fig. 6. The data fit well to a single exponential function with a rate constant of 0.10 $\pm$ 0.01 s^{-1} and a maximum of 0.89 $\pm$ 0.06 mol of P_i per mol of MIII. This rate constant is similar to the rate of ATP binding to the motor domain expected at 25 μM ATP, which suggests the reaction is limited by ATP binding to the motor domain. ATP hydrolysis by the kinase domain may be much slower so that it fails to contribute to the reaction under these conditions. The maximum amount of ATP hydrolyzed per myosin (burst) was used to estimate the equilibrium constant for ATP hydrolysis ($K_3 = 9$) using the following equation: burst $= K_3/(1 + K_3)$.

Binding to Pyrene Actin Filaments—We examined the binding of MIII to pyrene actin filaments in the strong binding states (ADP and nucleotide-free) with a fluorescence titration experiment. We measured the degree of quenching of 0.1 μM pyrene actin with varying concentrations of myosin III to determine the actin binding affinity in the presence and absence of ADP. The amplitudes of the fluorescence decrease were plotted as a function of MIII concentration and fit to the quadratic equation to determine the dissociation constant for binding to actin in the presence ($1/K_{10} = 0.06 \pm 0.03$ μM) and absence of ADP ($1/K_6 = 0.06 \pm 0.02$ μM). The degree of pyrene actin quenching was lower in the presence of ADP compared with nucleotide-free conditions (29 $\pm$ 2 and 39 $\pm$ 2%, respectively).

We also examined the binding of myosin III to pyrene actin filaments by examining the rates of association and dissociation in the presence of ADP and absence of nucleotide (Reaction 4) (Fig. 7).

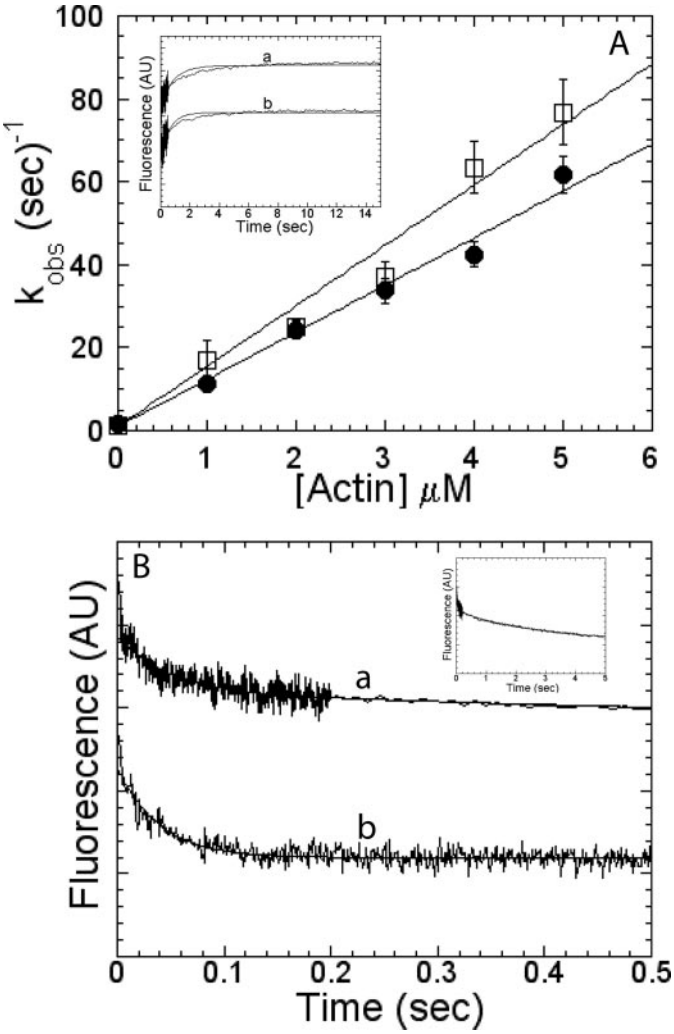

FIGURE 7. **Binding of myosin III to pyrene actin filaments.** *A,* pyrene fluorescence quenching upon mixing myosin III with 5–10-fold excess pyrene actin was fit to a single exponential function at each pyrene actin concentration in the absence of nucleotide (*closed circles*) and a two-exponential function in the presence of ADP (*open squares*). The rate of pyrene actin fluorescence quenching in the absence of nucleotide and the fast phase in the presence of ADP were linearly dependent on pyrene actin concentration. *Inset,* the rate of dissociation of myosin III from pyrene actin was determined by mixing 0.25 μM pyrene actomyosin III with 40-fold molar excess unlabeled actin filaments in the presence (*trace a,* $k_{obs} = 1.4 \pm 0.3$ and 0.18 ± 0.02 s^{-1}) and absence (*trace b,* $k_{obs} = 1.5 \pm 0.1$ s^{-1}) of 1 mM ADP. *B,* time courses of the fluorescence decrease upon binding pyrene actin to myosin III and the fit of the data: *trace a,* 0.4 μM MIII and 2 μM pyrene actin ($k_{obs} = 24.2 \pm 0.89$ s^{-1}); *trace b,* 0.4 μM MIII and 2.0 μM pyrene actin and 1 mM ADP ($k_{obs} = 21.5 \pm 1.3$ and 0.40 ± 0.03 s^{-1}; amplitudes = 0.6 and 0.4, respectively).

$$A^* + M \underset{}{\overset{K_6}{\longleftrightarrow}} AM$$

$$A^* + M \cdot ADP \overset{K_{10}}{\longleftrightarrow} AM \cdot ADP$$

REACTION 4

The association rates were determined by mixing MIII with varying concentrations of pyrene actin (at least 5-fold excess of MIII). In the absence of nucleotide the transients were fit to a single exponential function at each actin concentration meas-

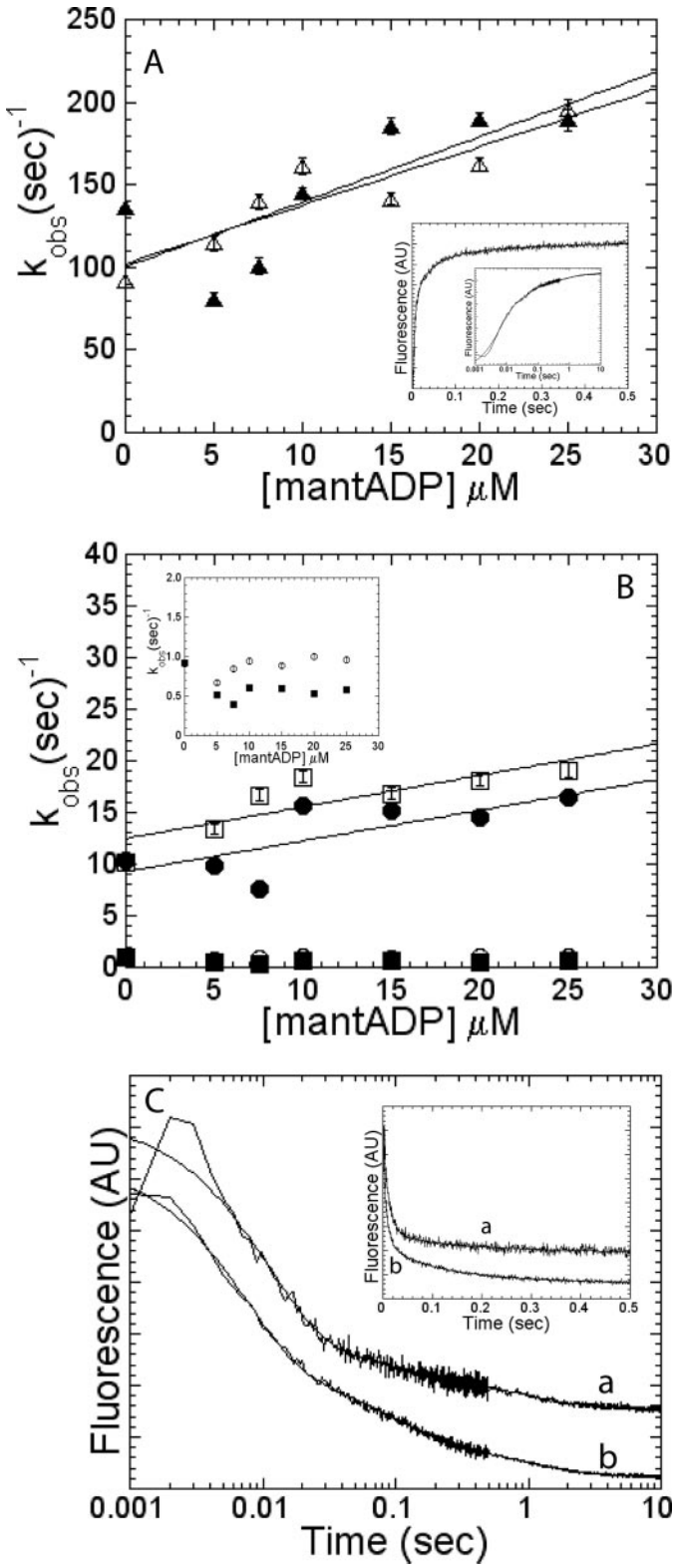

FIGURE 8. **Mant-ADP binding to myosin III and actomyosin III.** The rate of mant-ADP binding was measured by monitoring the fluorescence enhancement of mant-ADP upon binding to myosin (0.5 μM) or actomyosin III (0.5 μM MIII and 2.5 μM actin). The fluorescence transients were triphasic at each mant-ADP concentration. *A,* fast phase was linearly dependent on mant-ADP concentrations and similar in the presence (*closed triangles*) and absence (*open triangles*) of actin. *Inset,* transient from mixing 0.5 μM myosin III with 20 μM mant-ADP with the first 500 ms shown as well as the full 10 s. Trace was plotted on a log time scale (k_{obs} = 189 ± 4, 16.5 ± 0.4, and 0.53 ± 0.02 s^{-1}, amplitudes = 0.66. 0.26, 0.08, respectively). *B,* the rate of the intermediate phase was also dependent on mant-ADP concentration and similar in the presence (*closed circles*) and absence (*open squares*) of actin. The *inset* shows the slow phase that was independent of mant-ADP concentration and slightly lower in the presence (*closed squares*) compared with the absence (*open circles*) of actin. *C,* rate of dissociation of mant-ADP from myosin III and actomyosin III was monitored by mixing myosin III (0.5 μM) or actomyosin III (0.5 μM MIII, 2.5 μM actin) in the presence of 12.5 μM mant-ADP with 5 mM ATP. The fluorescence transients of actomyosin and myosin III were fit to a triexponential function. The fluorescence transients are shown on a log time scale. The *inset* shows the first 500 ms of the trace on a linear scale (myosin III, *trace a,* k_{obs} = 92 ± 3, 10.2 ± 1.6, and 0.91 ± 0.08 s^{-1}; amplitudes = 0.78, 0.11, and 0.11, respectively. Actomyosin III, *trace b,* k_{obs} = 136 ± 2, 10.4 ± 0.2, and 0.92 ± 0.03 s^{-1}; amplitudes = 0.67, 0.23, and 0.10, respectively).

ured. The association rates were fit to a two-exponential function in the presence of ADP, a slow phase that was independent of actin concentration in the concentration range measured (k_{obs} ~ 0.2–0.4 s^{-1}) and a fast phase that was dependent on actin concentration (relative amplitudes, slow = 0.44 and fast = 0.56). The rate of the fast phase of myosin III binding to actin was similar in the presence of ADP (k_{+10} = 14.6 ± 0.6 μM^{-1}·s^{-1}) compared with the rate of binding in the absence of nucleotide (k_{+6} = 11.4 ± 0.6 μM^{-1}·s^{-1}). The rate of dissociation from actin was monitored by mixing pyrene actomyosin III with excess unlabeled actin filaments. The dissociation rates were fit to a single exponential function in the absence of ADP (k_{-6} = 1.5 ± 0.1 s^{-1}, respectively) and double exponential function in the presence of ADP (k_{-10} = 1.4 ± 0.3 s^{-1} and 0.18 ± 0.02; relative amplitudes, 0.35 and 0.65, respectively). Thus, the affinity of myosin III for pyrene actin, calculated from the dissociation and association rate constants, was found to be similar in the presence and absence of ADP ($1/K_6$ = 0.13 ± 0.01 μM and $1/K_{10}$ = 0.08 ± 0.01 μM), which is in fairly good agreement with the titration experiments.

ADP Binding to and Dissociation from Myosin and Actomyosin III—The rate of ADP binding to myosin III (0.5 μM) and actomyosin III (0.5 μM MIII; 2.5 μM actin) was monitored with mant-ADP (Reaction 5) (Fig. 8).

$$\mathrm{M} + \mathrm{mADP} \overset{K_{5B}}{\longleftrightarrow} \mathrm{M \cdot mADP^*} \overset{K_{5A}}{\longleftrightarrow} \mathrm{M \cdot mADP'^*}$$

$$\mathrm{AM} + \mathrm{mADP} \overset{K_{5B}'}{\longleftrightarrow} \mathrm{AM \cdot mADP^*} \overset{K_{5A}'}{\longleftrightarrow} \mathrm{AM \cdot mADP'^*}$$

REACTION 5

There was a triphasic transient observed upon mant-ADP binding to myosin or actomyosin III (Fig. 8*A*). In the presence and absence of actin, the fast and intermediate phases were dependent on mant-ADP concentrations (Fig. 8, *A* and *B*). The data were modeled as a single step binding to the kinase domain and a two-step binding to the motor domain, in which the mant-ADP fluorescence was sensitive to both states (see rationale below). In the absence of actin the linear dependence of fast and intermediate phases on mant-ADP concentration allowed us to determine the second-order binding constants for each phase (fast phase = 3.5 ± 0.7 μM^{-1}·s^{-1}, intercept of 102 ± 10 s^{-1}, intermediate phase = 0.31 ± 0.09 μM^{-1}·s^{-1} with an intercept of 12.5 ± 1.3 s^{-1}). In the presence of actin, the two phases were

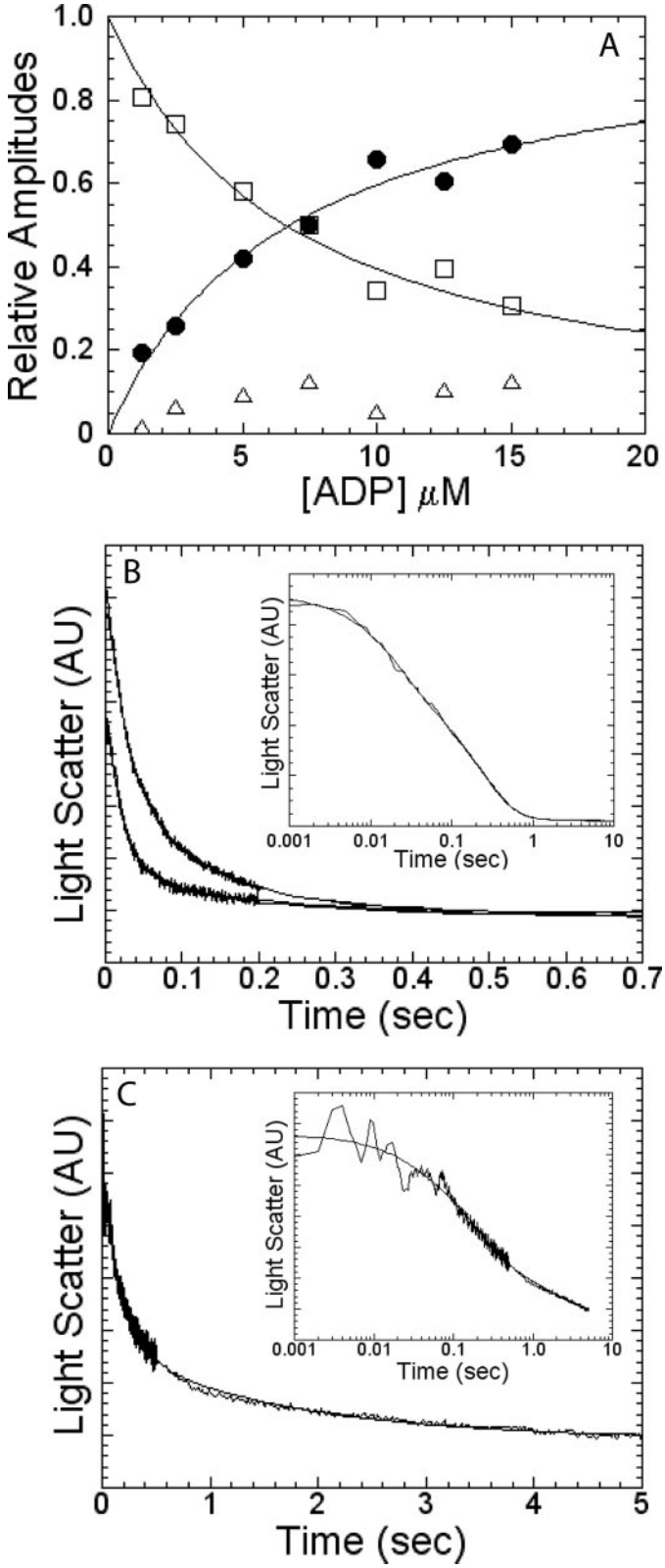

FIGURE 9. **ADP binding to and dissociation from actomyosin III.** *A,* 0.5 μM actomyosin III in the presence of varying concentrations of ADP was mixed with 5 mM ATP. The fast phase was equivalent to the rate of ATP-induced dissociation in the absence of nucleotide, and the two slower phases were modeled to be the rate of ADP release prior to ATP binding. The intermediate and slow phases were found to be 5–10 and 0.5–2 s^{-1}, respectively, whereas the fast phase was 40–70 s^{-1} at each ADP concentration. The amplitude of the intermediate phase (*open squares*) increased similarly dependent on mant-ADP concentrations (fast phase = 3.9 ± 1.4 $\mu M^{-1}\cdot s^{-1}$, intercept of 100 ± 20 s^{-1}, intermediate phase = 0.35 ± 0.16 $\mu M^{-1}\cdot s^{-1}$, intercept of 9.3 ± 1.7 s^{-1}). The slow phase in the absence and presence of actin was independent of mant-ADP concentration in the concentration range measured (0.88 ± 0.12 and 0.54 ± 0.08 s^{-1}, respectively) (Fig. 8*B*, *inset*). The amplitudes of each of the fast, intermediate, and slow phases were similar at each mant-ADP concentration in the absence (relative amplitudes = 0.63, 0.25, and 0.12) and presence (relative amplitudes = 0.60, 0.29, and 0.11) of actin.

The rate of mant-ADP release from myosin III and actomyosin III was determined by mixing actomyosin (0.5 μM MIII; 2.5 μM actin) or myosin III (0.5 μM) in the presence of 12.5 μM mant-ADP with 5 mM ATP (Fig. 8*C*). The rate of mant-ADP release from myosin III and actomyosin III was also triphasic. The fast and intermediate phases in the absence (92 ± 3 and 10.1 ± 1.6) and presence (136 ± 2 and 10.4 ± 0.2) of actin were fairly consistent with the *y* intercept determined from the direct binding experiments described above. The slow phase was found to be similar in the absence (0.91 ± 0.08 s^{-1}) and presence (0.92 ± 0.03 s^{-1}) of actin. The relative amplitudes of the fast, intermediate, and slow phases were slightly different in the absence (0.78, 0.11, and 0.11) and presence of actin (0.67, 0.23, and 0.10). The intermediate and slow mant-ADP release rates in the presence of actin are in reasonably good agreement with the release of unlabeled ADP from actomyosin III measured with light scatter (Fig. 9). Thus, the intermediate and slow phases were modeled to be ADP binding to and release from the motor domain, and the fast phase was modeled to be ADP binding to and release from the kinase domain.

We analyzed the two-step mant-ADP binding to the motor domain of myosin and actomyosin III with equations outlined in Henn and De La Cruz (37). This model incorporates the measured slow and fast phases for mant-ADP binding and dissociation as well as the amplitudes of the each of these phases to determine the rate constants and equilibrium constants for the two-step process. The overall affinity for mant-ADP can also be determined. Our data fit reasonably well to this kinetic model, with a few exceptions (see below), and the determined rate and equilibrium constants are shown in Table 2. The calculated dissociation constants for the overall affinity for mant-ADP were quite similar in the presence and absence of actin (K_d (overall) = and 22 ± 7 and 14 ± 7 μM, respectively). The rates of association of the slow phase are slightly reduced (Fig. 8*B*, *inset*; and 0.4–0.6 and 0.7–1.0 s^{-1} in the pres-

as a function of ADP concentration, whereas the amplitude of the fast phase (*closed circles*) decreased. The dependence of the amplitude of the fast/intermediate phases were fit to a hyperbola to determine the dissociation constant for ADP binding to the myosin III motor domain ($1/K_{5B}' = 6.7 \pm 0.5$ μM). The amplitude of slow phase (*open triangles*) was ~10% of the overall signal. *B,* three-phase fluorescence transient was observed upon mixing 0.5 μM actomyosin in the presence of 1.25 μM ADP (*bottom trace*, k_{obs} = 35.56 ± 1.0, 6.2 ± 2.0, and 0.9 ± 0.1 s^{-1}) or 5 μM ADP (*top trace*, k_{obs} = 48.83 ± 0.5, 4.5 ± 0.1, and 0.36 ± 0.08 s^{-1}) with 5 mM ATP. The *inset* shows the 5 μM ADP trace on a log scale. *C,* ADP release was measured as described above, but at a higher actin concentration to populate the AM·ADP′ state. The light scatter transient of actomyosin III (0.5 μM MIII, 2.5 μM actin) was best fit to a three-exponential function in the presence of 25 μM ADP and 5 mM ATP (k_{obs} = 40 ± 9, 5.4 ± 0.5, 0.6 ± 0.1 s^{-1}; relative amplitudes = 0.12, 0.57. 0.31, respectively). *Inset* shows the entire 10-s trace plotted on a log scale.

ence and absence of actin, respectively) compared with what is expected from the model (1.0–1.2 and 1.1–1.4 s^{-1} in the presence and absence of actin, respectively). The ratio of the amplitudes of the slow and intermediate phases for mant-ADP dissociation are in good agreement with the determined equilibrium constant (K_{5A}) for the transition between the two proposed ADP states in the presence and absence of actin ($K_{5A}' = 1.8$, dissociation amplitude ratio (slow phase/intermediate phase) ~2.4; $K_{5A} = 1.1$, dissociation amplitude ratio ~1.0). However, the amplitudes from the mant-ADP association experiments are slightly different from what is expected from the two-state model in the presence and absence of actin (association amplitude ratio ~2.7 and ~2.2, respectively).

We also examined the rate of ADP release from actomyosin III by performing ATP-induced dissociation experiments with 0.5 μM actomyosin III in the presence of varying concentrations of ADP (Reaction 6) (Fig. 9, *A* and *B*).

$$\begin{array}{l} \overset{K_1'}{\qquad} \overset{K_2'}{\qquad} \overset{K_8'}{\qquad} \\ \mathrm{AM} + \mathrm{ATP} \leftrightarrow \mathrm{AM(ATP)} \leftrightarrow \mathrm{AM \cdot ATP} \leftrightarrow \mathrm{AM \cdot ATP} \\ \quad + \\ \quad \mathrm{ADP} \\ K_{5B}' \Updownarrow \\ \mathrm{AM \cdot ADP} \\ K_{5A}' \Updownarrow \\ \mathrm{AM \cdot ADP'} \end{array}$$

REACTION 6

The light scatter transients contained three phases as follows: a fast phase equivalent to the rate of ATP-induced dissociation (30–70 s^{-1}), an intermediate phase (5–10 s^{-1}), and a slower phase (0.5–2.0 s^{-1}) that was a small percentage (5–10%) of the overall amplitude. The amplitudes of the fast and intermediate phases were dependent on ADP concentration. The plot of the relative amplitudes as a function of ADP concentration fit well to the hyperbolic curve, with an ADP affinity of 6.8 ± 0.4 μM (Fig. 9*A*). A similar analysis was performed with pyrene actin, but the ADP affinity was found to be ~36 μM (data not shown). We propose that the slow phase monitors the transition out of the AM·ADP′ state, but because this state may have a relatively low affinity for actin ($K_d \sim 5$ μM), the amplitude of this phase was quite small (see Fig. 9*C* for experiments at a higher concentration of actin). Our analysis of the intermediate phase likely measures the interaction of ADP with actomyosin (K_{5B}') and refers to the ADP affinity of the AM·ADP′ state.

We also measured the rate of ADP release as described above but in the presence of 2.5 μM actin (Fig. 9*C*). The light scatter transients were best fit to three exponentials with two of the phases similar to that described above ($k_{obs} = 40 \pm 10$ and 5.4 ± 0.5 s^{-1}) and the slow phase similar to the k_{cat} and slow phase of mant-ADP dissociation ($k_{obs} = 0.6 \pm 0.1$ s^{-1}). The relative amplitudes of the slow and intermediate phases were similar to the mant-ADP release amplitudes of these phases in the presence of actin (0.65 for the 5.4 s^{-1} phase and 0.35 for the 0.6 s^{-1} phase). Similar results were obtained by monitoring pyrene actin (5 μM pyrene actin, 0.5 μM MIII) fluorescence (k_{obs} = 67.5 ± 11, 5.3 ± 0.4, and 0.52 ± 0.12, relative amplitudes of the two slower phases 0.67 and 0.33, respectively) (data not shown).

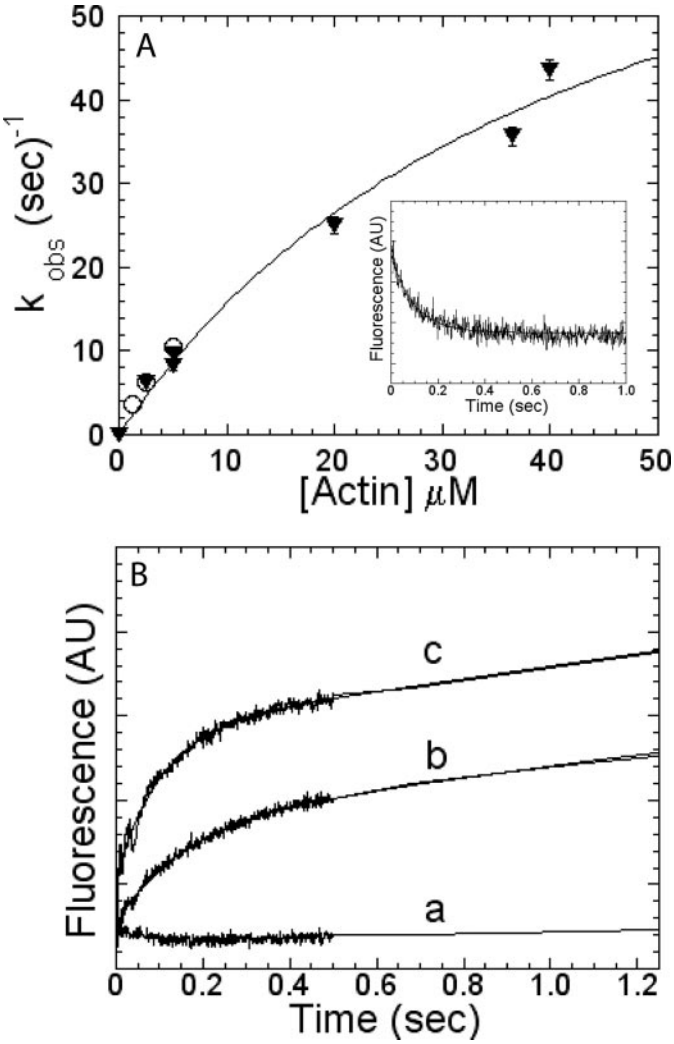

FIGURE 10. **Phosphate release from myosin III and actomyosin III.** The rate of phosphate release was monitored by mixing 2 μM MIII with 1.75 μM ATP, aging the reaction for 5 s, and then mixing with phosphate-binding protein in the presence and absence of actin. *A*, rate of the phosphate burst was dependent on actin concentration (*closed triangles*). The hyperbolic fit of the data demonstrates a maximum rate of phosphate release of 85 ± 17 s^{-1} and an affinity for actin in the ADP·P_i state ($1/K_9$) of 44 ± 15 μM. The rate of pyrene actin quenching in the ADP·P_i state (*open circles*) was similar to the rate of phosphate release. MIII was mixed with 50 μM ATP, aged for 10 s, and then mixed with at least a 5-fold excess pyrene actin (*inset*, pyrene actin fluorescence transient with a $k_{obs} = 9.6 \pm 0.3$ s^{-1}; final conditions: 0.75 μM MIII, 25 μM ATP, and 5 μM pyrene actin). *B*, fluorescence transients of phosphate release in the presence and absence of actin. In the absence of actin, no phosphate burst was observed, and the linear transient was fit to the steady-state rate. In the presence of actin there was a burst phase followed by a linear phase. The data were fit to a single exponential function with a steady-state to determine the rate of phosphate release at each actin concentration. Final reaction conditions were as follows: 1 μM MIII, 0.85 μM ATP, 2.65 μM phosphate-binding protein, and 0 μM actin (*transient a*), 2.5 μM actin (*transient b*, k_{obs}(burst) = 6.3 ± 0.2 s^{-1}), and 5 μM actin (*transient c*, k_{obs}(burst) = 9.7 ± 0.3 s^{-1}).

Phosphate Release—We examined the rate of actin-activated phosphate release using a sequential mix experiment described under "Experimental Procedures" (Reaction 7) (Fig. 10).

$$\mathrm{M \cdot ADP \cdot P_i} + \mathrm{A} \overset{K_9}{\leftrightarrow} \mathrm{A^*M \cdot ADP \cdot P_i} \overset{K_4'}{\leftrightarrow} \mathrm{AM \cdot ADP} + \mathrm{P_i} \overset{K_5'}{\leftrightarrow} \mathrm{AM \cdot ADP}$$

REACTION 7

The rate of phosphate release in the presence and absence of actin was determined by mixing 2 μM myosin III with 1.75 μM ATP, allowing the reaction to age for 5 s, and then mixing with phosphate-binding protein and various concentrations of actin (0–40 μM). A standard curve with inorganic phosphate allowed us to determine the concentration of phosphate release during the reaction. Because ATP binding is slow and the equilibrium constant for hydrolysis is high in myosin III, we calculated that ~0.05 μM myosin III would be in the ADP·P_i state after the aging time, and the remainder would be in the nucleotide-free and myosin ATP states. In the absence of actin there was no phosphate burst observed, and a linear fit of the transient was found to be similar to the steady-state ATPase rate expected at this ATP concentration (0.005 mol of P_i·mol of myosin^{-1}·s^{-1}). In the presence of actin, a burst was seen followed by a linear phase (Fig. 10*B*). The burst rate was plotted as a function of actin concentration and fit to a hyperbolic relationship, to determine the maximum rate of phosphate releases ($k_{+4}' = 85 \pm 17$ s^{-1}) and affinity for actin in the ADP·P_i state ($1/K_9 = 44 \pm 15$ μM) (Fig. 10*A*). It is possible to fit the phosphate release rates to a linear function in the actin concentration range measured. However, the results would not dramatically affect the conclusion that phosphate release is rapid and the affinity for actin in the ADP·P_i state is weak ($k_{+4}' \geq 85 \pm 17$ s^{-1} and $1/K_9 \geq 44 \pm 15$ μM). The amplitude of the burst phase corresponded to a phosphate burst of 0.05 μM P_i at 40 μM actin, which was in good agreement with our expectations based on the predicted amount of myosin III in the ADP·P_i state at the end of the 5-s age time. The linear phase was also in good agreement with the steady-state ATPase rate at 0.875 μM ATP.

Weak-to-Strong Transition—We examined the rate of formation of the strongly bound actomyosin III complex using pyrene-labeled actin. MIII was mixed with 50 μM ATP, aged for 10 s, and mixed with varying concentrations of pyrene actin (at least 5-fold greater than the MIII concentration). The fluorescence decrease followed a single exponential and was dependent on actin concentration (Fig. 10*A*, *inset*). The rate of pyrene fluorescence quenching was plotted as a function of actin concentration and compared with the phosphate release data (Fig. 10*A*). The comparison demonstrates that the rate of pyrene fluorescence quenching was nearly identical to the rate of phosphate release at each actin concentration measured (1.25, 2.5, and 5 μM actin).

DISCUSSION

Catalytic Cycle of the Myosin III Kinase Domain—The overall rate of the kinase autophosphorylation reaction was quite slow compared with the motor ATPase cycle (0.002 s^{-1} in the presence of 200 μM ATP; Fig. 3*C*). Interestingly, the rate of autophosphorylation, measured by phosphothreonine incorporation, was linearly dependent on ATP concentrations up to 1 mM ATP. Thus, a step in the kinase reaction that is dependent on ATP binding may be rate-limiting at physiological ATP concentrations. Direct binding experiments with mant-ATP indicate that ATP binding to the kinase domain is much faster than ATP binding to the motor domain. If the motor domain adopts a conformation in the presence of ATP that favors phosphorylation, ATP binding to the motor domain could limit the rate of autophosphorylation. The slow steady-state ATPase rate of the kinase domain indicates the myosin III kinase domain does not turn over rapidly without phosphorylating its substrate, as observed in some PAK1 kinases (24). The mant-ADP release experiments demonstrate ADP release from the kinase domain is rapid and not likely to be rate-limiting. The experiments with mant-ATP and mant-ADP suggest the kinase domain has a 2-fold higher affinity for ATP compared with ADP ($K_d \sim 10$ and ~20 μM, respectively), and thus ADP is not likely to inhibit ATP binding under physiological conditions (mM ATP and μM ADP). The relative affinities for ATP and ADP may be altered by the mant fluorophore. Indeed, the reduced autophosphorylation levels with mant-ATP indicate mant-ATP binds weaker than ATP. Further detailed analysis of the kinetics of the kinase domain reaction cycle will be evaluated in future studies.

Our kinase autophosphorylation experiments demonstrate that ~2 mol of phosphate are incorporated into myosin III when autophosophorylation is complete, which is similar to the results of Komaba *et al.* (19). Komaba *et al.* (19) suggest that both threonine and serine residues are phosphorylated in myosin III, so there may be one phosphoserine and one phosphothreonine in the motor domain. Also, because the Western blotting and radioactivity measurements can only detect an increase in phosphorylation, we have not addressed the possibility of myosin III becoming phosphorylated during the expression and purification process. Interestingly, the rate of phosphothreonine incorporation measured by Western blotting was ~2-fold faster than the rate of total phosphorylation measured by radioactivity. Thus, the kinase domain may phosphorylate threonine more rapidly than serine in myosin III. A more detailed study will determine the exact number, location, and rate of phosphorylation of the phosphorylatable serine and threonine residues.

It is intriguing to speculate that kinase autophosphorylation regulates the motor activity of myosin III. Komaba *et al.* (19) suggest the myosin III motor is not regulated by autophosphorylation. However, a fish myosin IIIA construct lacking the N-terminal kinase domain moved more efficiently than wild-type myosin III to the tips of filopodia in HeLa cells (40). In addition, the human and fish myosin III construct lacking the kinase domain localized more efficiently to the tips of hair cell stereocilia (41). Future studies will evaluate the possibility of kinase-dependent regulation of the motor, by examining the kinetics of a kinase deleted and/or inactivated construct.

General Properties of the Myosin III Motor ATPase Cycle—We were able to measure most of the rate and equilibrium constants in myosin III motor domain ATPase cycle. The kinase domain activity was well separated from the motor activity in both the steady-state and transient kinetic experiments. The myosin III motor has a slow maximum rate of actin-activated ATPase ($k_{cat} = 0.77 \pm 0.08$ s^{-1}) and relatively high K_{ATPase} (34 ± 11 μM) compared with processive myosins such as myosin V and VI (20, 38), suggesting myosin III has a low duty ratio. However, actin co-sedimentation assays demonstrate myosin III has a relatively high steady-state affinity for actin ($K_{actin} = 7$ μM), which suggests it is a high to intermediate duty ratio motor. We found that myosin III has a

fast rate of actin-activated phosphate release ($k_4' = 85 \pm 17$ s^{-1}). Also, ADP release measured by ATP-induced dissociation in the presence of ADP was biphasic ($k_{+5A}' = 0.6 \pm 0.1$ s^{-1} and $k_{+5B}' = 6.8 \pm 0.2$ s^{-1}). We propose that the rate-limiting step in the myosin III ATPase cycle is a transition between two actomyosin-ADP states (K_{5A}'). We also propose the predominant steady-state intermediate in the myosin III ATPase cycle is a unique actomyosin-ADP state that has an affinity for actin in the micromolar range ($K_d \sim 5$ μM), instead of the usual nanomolar range of most myosin motors. The slow transition between actomyosin-ADP states that limits the overall reaction of the myosin III ATPase cycle may allow myosin III to stay associated with the actin bundles, such as are present in the calycal processes of the photoreceptors and stereocilia of the inner ear hair cells.

Structural Basis for Slow ATP Binding to the Motor Domain—Myosin III has a very slow rate of ATP binding both in the presence and absence of actin. The rate of binding is similar to that of myosin VI (38–39, 42). The reduction in ATP binding could be a result of a reduction in the initial interaction between ATP and myosin (K_1) or the isomerization step (K_2) to form a tight stereospecific interaction with ATP. The isomerization step was determined from the maximum rate of the hyperbolic fit of the ATP-induced dissociation data (Fig. 5*A*). However, because the data are close to being linearly dependent on ATP concentration, there is some uncertainty in the maximum rate (k_{+2}'). Nevertheless, the hyperbolic fit of the ATP-induced dissociation data suggests that K_1' is the main step altered in myosin III, whereas K_2' is reduced 4-fold, compared with other myosin isoforms that have fast ATP binding. Indeed, myosin VI also has a reduced K_1' and K_2' compared with other myosin isoforms (38–39, 42). The structural basis for slow ATP binding in myosin VI is linked to an insert in the upper 50-kDa domain (42). This insert appears to interact with and alter the dynamics of switch I, one of the nucleotide-binding elements in myosin. Sequence alignments with myosin VI indicate that myosin III also has a sequence that is divergent from other myosins in this region suggesting a similar structural mechanism may be responsible for the reduced rate of ATP binding. In addition, a recent paper (43) suggested amino acid sequence differences in this same region may account for the 5-fold reduced ATP binding rate observed in myosin Vb compared with myosin Va. Overall, differences in this region may result in the variability in ATP binding throughout the myosin superfamily.

Another possible structural mechanism for slow ATP binding to the myosin III motor is that the presence of the kinase domain may sterically interfere with nucleotide binding to the motor. The kinase domain is located at the N terminus, which may be in close enough proximity to the active site to interfere with ATP binding. It is possible that myosin III exists in two or more conformations, of which one has a reduced ATP binding rate. We did not obtain evidence for more than one conformation of myosin or actomyosin III from our mant-ATP binding and ATP-induced dissociation experiments. However, the rate of ATP binding was enhanced ~10-fold in presence of actin (Fig. 4*C*), suggesting actin binding induces a conformation that is more favorable for ATP binding. Further studies will investigate the structural mechanism of slow ATP binding and determine its physiological role in the cell.

Myosin III Motor ATPase Cycle in the Absence of Actin—The rate-limiting step in the myosin III ATPase cycle in the absence of actin is likely phosphate release as is the case for most of the myosins that have been kinetically characterized (8). Although we did not directly measure the rate of ATP hydrolysis, we found that the equilibrium constant for ATP hydrolysis is quite high ($K_3 = 9$). Kinetic simulations suggest the rate of ATP hydrolysis must be at least 0.5 s^{-1} to account for the ATP hydrolysis data (calculated at 25 μM ATP, $K_1k_{+2} = 0.1$ s^{-1}, $K_3 = 9$, and $k_{+4} = 0.07$ s^{-1}). ADP release (1.0 ± 0.2 s^{-1}) is nearly 10-fold faster than the steady-state rate. This suggests that the predominant steady-state intermediate is the myosin ADP·P_i state because although ATP binding is slow, hydrolysis is favored and phosphate release is rate-limiting. Thus, actin binding is required to activate the phosphate release step and the catalytic cycle of myosin III, as is the case with many myosin motors that have been kinetically characterized to date (2, 7, 8).

Myosin III Motor ATPase Cycle in the Presence of Actin—In contrast to the absence of actin, phosphate release is not rate-limiting in the presence of actin. In fact, phosphate release is quite rapid in the presence of actin and similar to that of other high duty ratio myosins ($k_4' = 85 \pm 17$) (20, 37, 39). The slow phase from the mant-ADP release ($k'_{+5A} = 0.97 \pm 0.02$ s^{-1}) and ADP release ($k'_{+5A} = 0.6 \pm 0.1$ s^{-1}) experiments were similar to the maximum steady-state ATPase rate ($k_{cat} = 0.77 \pm 0.08$). Our results indicate there are two different actomyosin-ADP states, and the transition between those states is slow and rate-limiting. Other myosins have been shown to have a rate-limiting transition between actomyosin-ADP states (37, 44). Our results demonstrate the first actomyosin-ADP state (AM·ADP′) immediately following phosphate release is more populated at higher actin concentrations, which is consistent with this state containing an intermediate affinity for actin. This intermediate actin affinity state was not seen in the steady-state pyrene actin titration experiments, which indicates the AM·ADP′ state that contains 50-fold higher actin affinity dominated in these experiments. Two phases were seen when we examined the direct binding of myosin III to pyrene actin in the presence of ADP, providing additional evidence for two myosin·ADP states. The mant-ADP experiments also provide evidence for two myosin·ADP states and allowed us to determine the equilibrium between the two myosin·ADP states (see discussion below and Scheme 2).

The K_{ATPase} can be calculated from the following rate and equilibrium constants in myosins with rate-limiting ADP-release (20, 45): $K_{ATPase} = k_5'/\{(k_4'/1/K_9)\ [K_3/(K_3 + 1)]\}$. Assuming that ADP release is the rate-limiting step in myosin III, the calculated K_{ATPase} would be 0.44 μM actin, which is ~100-fold lower than the measured K_{ATPase} (34 ± 11 μM). Because the AM·ADP′ state has a weaker than normal affinity for actin ($K_{10A} \sim 5$ μM), this equation does not fit well to our ATPase data. However, kinetic simulations using the measured rate and equilibrium constants and including two ADP states, with the AM·ADP′ state exhibiting a 5 μM affinity for actin, fit the steady-state actin binding data quite well

(Fig. 2*B*). The duty ratio can be calculated using the assumption that it is equal to the rate of formation of the strong binding states divided by the addition of the rate of formation plus the rate of loss of the strong binding states. At high actin concentrations the following rate constants can be used to describe the duty ratio: $(k_{+4}'/(k_{+4}' + k_{5A}) = 85/(85 + 0.77))$, which gives a value close to 1. This conclusion is in reasonably good agreement with the steady-state actin binding data, which reaches a maximum fraction bound of 0.91 ± 0.1.

The mant-ADP binding and dissociation data demonstrate the equilibrium constant between the two myosin·ADP states is similar in the presence and absence of actin, suggesting weak coupling between the actin and nucleotide-binding sites with ADP (Scheme 2).

$$K_{5A}' = 1.8$$

$$\text{AM} \cdot \text{ADP}' \leftrightarrow \text{AM} \cdot \text{ADP}$$

$$\Updownarrow K_d \sim 5\,\mu\text{M} \qquad \Updownarrow K_d = 0.1\,\mu\text{M}$$

$$\text{M} \cdot \text{ADP}' \leftrightarrow \text{M} \cdot \text{ADP}$$

$$K_{5A} = 1.1$$

SCHEME 2

However, because our model proposes a large difference between the actin affinities of these two states, the scheme is not energetically balanced. This may be caused by additional intermediates and/or side reactions within the pathway. Alternatively, a third myosin·ADP state may be populated, which has a 50-fold higher equilibrium constant in the presence compared with the absence of actin. This model would make it less likely for myosin III to proceed through a dissociative pathway (dissociate from actin following phosphate release and rapidly release ADP).

We also determined that the rate of pyrene fluorescence quenching when mixing myosin III in the ADP·P_i state with actin was identical to the rate of phosphate release. Thus, even though the AM·ADP′ state has an intermediate affinity for actin, it still quenches pyrene actin. This is surprising because typically only strong binding conformations of myosin can quench pyrene actin (see exceptions below). Myosin III appears to have a weaker affinity for actin in the strong binding states than other myosins as a result of a faster than normal rate of dissociation from actin (~1 s^{-1} in ADP and rigor) (see Table 2). The affinity for actin in the ADP and rigor states is ~100 nM which is 10–100-fold weaker than most other myosins in these states (8). Thus, the intermediate affinity of the AM·ADP′ state may be a result of a faster than typical dissociation rate that weakens its affinity for actin even though it still forms a specific interaction with actin that can quench pyrene actin.

Actomyosin-ADP States—Rosenfeld and Sweeney (46) have proposed a two-step ADP release in myosin V in which the first step has an intermediate affinity for actin and the second step has a high affinity for actin (Scheme 3).

$$\underset{\text{"Weak"}}{\text{A*M} \cdot \text{ADP} \cdot \text{P}_i} \overset{K_4'}{\longleftrightarrow} \underset{\text{"Intermediate"}}{\text{AM} \cdot \text{ADP}' + \text{P}_i} \overset{K_{5A}'}{\longleftrightarrow} \underset{\text{"Strong"}}{\text{AM} \cdot \text{ADP}}$$

SCHEME 3

The transition between these two actomyosin-ADP states (K_{5A}') is referred to as the weak-to-strong transition and is slower than the rate of phosphate release but faster than ADP release in myosin V. This transition that has been detected in several other myosins is accompanied by an additional lever arm swing (44, 46, 47, 49–51). In the case of smooth muscle myosin the actomyosin·ADP′ state with intermediate actin affinity does not quench pyrene actin (47). Myosin V was shown to have two ADP states that both quench pyrene actin. One of these states has a weak actin affinity (~0.5 μM), and the other has a strong actin affinity (~nM) (52). Jontes *et al.* (50) demonstrated that there are two actomyosin-ADP states in myosin I and that both of these states quench pyrene actin. However, the actin affinity of these two states has not been characterized. Myosin III is similar to myosin V in that it transitions into an intermediate affinity actomyosin·ADP′ state following phosphate release, and this state can quench pyrene actin. Thus, in the presence of higher actin concentrations the actomyosin·ADP′ state can form a stereospecific interaction with actin that can generate tension.

The transition between the two actomyosin-ADP states is thought to be a strain-sensitive step utilized by dimeric myosins to coordinate the catalytic cycles of each head of the dimer (20, 38, 39, 51). This allows the dimeric myosins to processively walk hand-over-hand along actin without diffusing away. However, myosin III is thought to be monomeric because it does not contain a predicted coiled-coil sequence and thus it is not clear what purpose strain sensitivity would serve. The walking mechanism of myosin III is currently unknown, but an additional actin-binding motif in the tail of myosin IIIA was identified (40). The long lived actomyosin·ADP′ state in myosin III with intermediate affinity for actin may allow myosin III to coordinate the conformational changes of the motor and the tail actin-binding motif, which may be necessary for it to walk along actin.

Other nonprocessive myosins such as smooth muscle myosin and non-muscle myosin IIB may use strain sensitivity to modulate force generation in response to the contractile needs of the cell (44, 47). Muscle myosins, which mainly bind to actin with a single head of the monomer, can exhibit strain sensitivity as a result of other myosin motors interacting with the same actin filament (48). Class I myosins, which are monomeric, have been shown to demonstrate strain sensitivity and an additional lever arm swing during ADP release (49, 50). Thus, strain sensitivity is also a characteristic of monomeric myosins and may be critical for myosins that function in actin networks or bundles in the cell.

Implications for the in Vivo Function of Myosin III—Myosin IIIA is primarily localized to the distal ends of actin-bundled structures such as the calycal processes in photoreceptors and stereocilia in inner ear hair cells (16, 41). In addition, myosin III in *Drosophila* was shown to be important for the transport of the signaling proteins arrestin and $G_q\alpha$, which are important for phototransduction (12, 13). The transport of arrestin was found to be

phosphatidylinositol phosphate-dependent, indicating that myosin III may be capable of binding lipids and transporting vesicles. Indeed the tail domain of myosin IIIA has been shown to bind phospholipids.[3] Thus, myosin III may be a cellular transporter capable of moving along actin bundles in sensory cells. The relatively high duty ratio of myosin III suggests it may function alone or in a small group of motors to transport proteins in the cell. Because myosin III contains an additional actin-binding site in its tail, it may have a unique walking mechanism that allows it to move processively along actin.

Altering the myosin III expression levels appears to alter the cytoskeletal structures of photoreceptor cells (53). The long lived actomyosin-ADP state may be important for mediating actin cross-linking dynamics and provide a mechanism to trigger actin cross-linking at specific actin concentrations in the cell. For example, at actin concentrations well above 5 μM, myosin III has a high duty ratio and would be a very efficient actin cross-linker, although at concentrations lower than 5 μM myosin III would be more likely to be dissociated from actin. However, the tail actin binding motif may prevent myosin III from completely dissociating at low actin concentrations.

While our paper was in review, another paper describing the kinetics of the human myosin IIIA motor domain, lacking the kinase domain and two IQ domains, was published (54). The results suggest ATP hydrolysis is rate-limiting, phosphate release is slow in the presence of actin, and the affinity for actin in the weak binding states is extremely high. These results appear to conflict with our results because we show phosphate release is rapid and the myosin·ADP·P_i state is relatively weak. We have examined actin-activated phosphate release of myosin III lacking the kinase domain but containing the two IQ domains, and we find that the phosphate release kinetics are identical to the results in Fig. 10 (data not shown). Thus, it is possible that removing the IQ domains significantly alters the kinetic properties of myosin III. Indeed, a study on myosin V demonstrated that altering the light chain of myosin V changes the kinetics of ATP hydrolysis (44).

In conclusion, we propose that myosin IIIA, which has a high to intermediate duty ratio, is kinetically tuned to provide two critical functions in the sensory cells. The observed duty ratio and long lived actomyosin-ADP state of myosin III may provide a mechanism for this motor to function as a cellular transporter in actin bundles. In addition, these kinetic features may allow myosin III to function as an actin cross-linker at higher concentrations of actin. Future studies will address the specific mechanism of myosin III walking/cross-linking and determine the regulation of its enzymatic and motile activities in the cell.

Acknowledgments—We thank Dr. Howard White for the generous gift of phosphate-binding protein. We thank Dr. Dan Safer and Dr. B. Ramamurthy for assisting with the acid quench studies. We also thank Dr. Michael Ostap and Dr. Enrique De La Cruz for critically reviewing and providing comments on the manuscript.

REFERENCES

1. Sellers, J. R. (2000) *Biochim. Biophys. Acta* **1496,** 3–22
2. Holmes, K. C., and Geeves, M. A. (1999) *Annu. Rev. Biochem.* **68,** 687–728
3. Brown, M. E., and Bridgman, P. C. (2003) *J. Neurobiol.* **58,** 118–130
4. Rayment, I., Rypniewski, W. R., Schmidt-Base, K., Smith, R., Tomchick, D. R., Benning, M. M., Winkelmann, D. A., Wesenberg, G., and Holden, H. M. (1993) *Science* **261,** 50–58
5. Dominguez, R., Freyzon, Y., Trybus, K. M., and Cohen, C. (1998) *Cell* **94,** 559–571
6. Coureux, P. D., Wells, A. L., Ménétrey, J., Yengo, C. M., Morris, C. A., Sweeney, H. L., and Houdusse, A. (2003) *Nature* **425,** 419–423
7. Sweeney, H. L., and Houdusse, A. (2004) *Philos. Trans. R. Soc. Lond. B Biol. Sci.* **359,** 1829–1841
8. De La Cruz, E. M., and Ostap, E. M. (2004) *Curr. Opin. Cell Biol.* **16,** 61–67
9. Montell, C., and Rubin, G. M. (1988) *Cell* **52,** 757–772
10. Porter, J. A., and Montell, C. (1993) *J. Cell Biol.* **122,** 601–612
11. Porter, J. A., Yu, M., Doberstein, S. K., Pollard, T. D., and Montell, C. (1993) *Science* **262,** 1038–1042
12. Lee, S. J., and Montell, C. (2004) *Neuron* **43,** 95–103
13. Cronin, M. A., Diao, F., and Tsunada, S. (2004) *J. Cell Sci.* **117,** 4797–4806
14. Dosé, A. C., and Burnside, B. (2000) *Genomics* **67,** 333–342
15. Dosé, A. C., and Burnside, B. (2002) *Genomics* **79,** 621–624
16. Dosé, A. C., Hillman, D. W., Wong, C., Sohlberg, L., Lin-Jones, J., and Burnside, B. (2003) *Mol. Biol. Cell* **14,** 1058–1073
17. Battelle, B.-A., Andrews, A. W., Calman, B. G., Sellers, J. R., Greenberg, R. M., and Smith, W. C. (1998) *J. Neurosci.* **18,** 4548–4559
18. Walsh, T., Walsh, V., Vreugde, S., Hertzano, R., Shahin, H., Haika, S., Lee, M. K., Kanaan, M., King, M., and Avraham, K. B. (2002). *Proc. Natl. Acad. Sci. U. S. A.* **99,** 7518–7523
19. Komaba, S., Inoue, A., Maruta, S., Hosoya, H., and Ikebe, M. (2003) *J. Biol. Chem.* **278,** 21352–21360
20. De La Cruz, E. M., Wells, A. L., Rosenfeld, S. S., Ostap, E. M., and Sweeney, H. L. (1999) *Proc. Natl. Acad. Sci. U. S. A.* **96,** 13726–13731
21. Mehta, A. (2001) *J. Cell Sci.* **114,** 1981–1998
22. Krementsov, D. N., Krementsova, E. B., and Trybus, K. M. (2004) *J. Cell Biol.* **164,** 877–886
23. Daniels, R. H., and Bokoch, G. M. (1999) *Trends Biochem. Sci.* **24,** 350–355
24. Wu, H., Zheng, Y., and Wang, Z. X. (2003) *Biochemistry* **42,** 1129–1139
25. Hiratsuka, T. (1983) *Biochim. Biophys. Acta* **742,** 496–508
26. Woodward, S. K., Eccleston, J. F., and Geeves, M. A. (1991) *Biochemistry* **30,** 422–430
27. Sweeney, H. L., Rosenfeld, S. S., Brown, F., Faust, L., Smith, J., Xing, J., Stein, L. A., and Sellers, J. R. (1998) *J. Biol. Chem.* **273,** 6262–6270
28. De La Cruz, E. M., Sweeney, H. L., and Ostap, E. M. (2000) *Biophys. J.* **79,** 1524–1529
29. Yengo, C. M., and Sweeney, H. L. (2004) *Biochemistry* **43,** 2605–2612
30. Sun, M., Oakes, J. L., Ananthanarayanan, S. K., Hawley, K. H., Tsien, R. Y., Adams, S. R., and Yengo, C. M. (2006) *J. Biol. Chem.* **281,** 5711–5717
31. Pardee, J. D., and Spudich, J. A. (1982) *Methods Enzymol.* **85,** 164–181
32. Pollard, T. D. (1984) *J. Cell Biol.* **99,** 769–777
33. White, H. D., and Rayment, I. (1993) *Biochemistry* **32,** 9859–9865
34. Yengo, C. M., De La Cruz, E. M., Safer, D., Ostap, E. M., and Sweeney, H. L. (2002) *Biochemistry* **41,** 8508–8517
35. Brune, M., Hunter, J. L., Corrie, J. E., and Webb, M. R. (1994) *Biochemistry* **33,** 8262–8271
36. White, H. D., Belknap, B., and Webb, M. R. (1997) *Biochemistry* **36,** 11828–11836
37. Henn, A., and De La Cruz, E. M. (2005) *J. Biol. Chem.* **280,** 39665–39676
38. Robblee, J. P., Olivares, A. O., and De La Cruz, E. M. (2004) *J. Biol. Chem.* **279,** 38608–38617
39. De La Cruz, E. M., Ostap, E. M., and Sweeney, H. L. (2001) *J. Biol. Chem.* **274,** 32373–32381
40. Erickson, F. L., Corsa, A. C., Dosé, A. C., and Burnside, B. (2003) *Mol. Biol. Cell* **14,** 4173–4180
41. Schneider, M. E., Dosé, A. C., Salles, F. T., Chang, W., Erickson, F. L., Burnside, B., and Kachar, B. (2006) *J. Neuroscience* **26,** 10243–10252
42. Menetrey, J., Bahloul, A., Wells, A. L., Yengo, C. M., Morris, C. A., Sweeney, H. L., and Houdusse, A. (2005) *Nature* **435,** 779–785

[3] A. C. Dosé, unpublished data.

43. Watanabe, S., Mabuchi, K., Ikebe, R., and Ikebe, M. (2006) *Biochemistry* **45,** 2729–2738
44. Rosenfeld, S. S., Xing, J., Chen, L., and Sweeney, H. L. (2003) *J. Biol. Chem.* **278,** 27449–27455
45. De La Cruz, E. M., Wells, A. L., Sweeney, H. L., and Ostap, E. M. (2000) *Biochemistry* **39,** 14196–14202
46. Rosenfeld, S. S., and Sweeney, H. L. (2004) *J. Biol. Chem.* **279,** 40100–40111
47. Rosenfeld, S. S., Xing, J., Whitaker, M., Cheung, H., Brown, F., Wells, A., Milligan, R. A., and Sweeney, H. L. (2000) *J. Biol. Chem.* **275,** 25418–25426
48. Nvitrai, M., and Geeves, M. A. (2004) *Philos. Trans. R. Soc. Lond. B Biol. Sci.* **359,** 1867–1877
49. Veigel, C., Coluccio, L. M., Jontes, J. D., Sparrow, J. C., Milligan, R. A., and Molloy, J. E. (1999) *Nature* **398,** 530–533
50. Jontes, J. D., Milligan, R. A., Pollard, T. D., and Ostap, E. M. (1997) *Proc. Natl. Acad. Sci. U. S. A.* **94,** 14332–14337
51. Whittaker, M., Wilson-Kubalek, E. M., Smith, J. E., Faust, L., Milligan, R. A., and Sweeney, H. L. (1995) *Nature* **378,** 748–751
52. Hannemann, D. E., Cao, W., Olivares, A., Robblee, J. P., and De La Cruz, E. M. (2005) *Biochemistry* **44,** 8826–8840
53. Lin-Jones, J., Parker, E., Wu, M., Dosé, A., and Burnside, B. (2004) *J. Cell Sci.* **117,** 5825–5834
54. Kambara, T., Komaba, S., and Ikebe, M. (2006) *J. Biol. Chem.* **281,** 37291–37301